

Scanning probe lithography: Application of organosilane self-assembled monolayers as ultra-thin resist films

Hiroyuki Sugimura

Department of Materials Science and Engineering, Kyoto University,
Sakyo, Kyoto 606-8501, Japan

TEL +81-75-753-9131

FAX +81-75-753-4861

E-mail: hiroyuki-sugimura@mtl.kyoto-u.ac.jp

URL: www.mtl.kyoto-u.ac.jp/groups/sugimura-g/index-E.html

Scanning probe lithography and molecular self-assembly have been integrated for constructing surface nanostructures. In the first part of this paper, organosilane monolayers grown through molecular self-assembly, i.e., self-assembled monolayers (SAMs), are applied as patterning media in scanning probe lithography based on scanning tunneling microscopy (STM) and atomic force microscopy (AFM) with an electrical conductive probe. The SAMs are successfully applied to resist films patternable in scanning probe lithography and etching masks for nanostructuring Si. Some of advanced techniques, that is, current-regulated AFM lithography, multilayer resist system and integration with photolithography, are presented as well. In the latter half, chemical methods to fabricate surface nanostructures are shown. Using SAM samples, on which nanopatterns formed by scanning probe lithography, as templates, minute objects including, organic molecules, nanoparticles and biomolecules are spatially arranged.

1. Introduction

Modern microscopy technologies, which enable to obtain enlarged images of minute objects, are close relations to lithographic technologies, in which mechanisms for generation and replication of micro ~ nanometer-scale patterns are required. Typical examples are the relation between optical microscopy and photolithography and that between electron microscopy and electron beam lithography. Thus, the development of microscopy has pushed the improvement of lithography's performance forward. Scanning probe microscopy (SPM) has been a powerful means to investigate material surfaces with high spatial resolutions at nanometer scales and, in favorable cases, at atomic ~ molecular scales. As well as other microscopes, SPM technologies have attracted much attention as nanoprocessing tools from their beginning and at present [1-8].

In order to apply SPM to nanolithography, the optimum resist material is a key factor. Among a variety of materials, organic thin films are practically important and have been frequently applied as patterning materials for lithography. Thus, the patterning of organic thin films by SPM is of special importance. However, in order to attain high spatial resolution in nanometer scale, resist films must be prepared in a thin and uniform layer. Furthermore, the films must be compatible with pattern transfer processes particularly with chemical etching.

In this review, we report on our research activities on scanning probe lithography using organosilane monolayers prepared on silicon substrates through a molecular self-assembling process. Such monolayers fulfill the requirements for high-resolution resist films including thickness, uniformity, patternability and compatibility to various pattern transfer processes and, therefore, are the most promising candidate for scanning probe lithography.

2. Organosilane SAMs prepared at the vapor/solid interface

The class of organic films known as self-assembled monolayer (SAM), spontaneously formed on certain substrates through chemisorption of organic molecules, have attracted considerable attention because of their structures with a highly ordered molecular arrangement and the simplicity of preparation processes [9]. Among various SAMs, organosilane SAMs formed on hydroxyl (OH)-bearing oxide surfaces through the chemical reaction of organosilane molecules with OH sites on the surfaces are promising for practical applications, since the organosilane SAMs are markedly stable mechanically and chemically due to the

strong immobilization through siloxane (Si-O-Si) bondings. Such organosilane SAMs were usually prepared at the liquid/solid interface by simply immersing a substrate in a solution of precursor molecules [10,11].

In this section, self-assembly of organosilane molecules at the vapor/solid interface is reported [12,13]. Besides the liquid phase process usually applied to SAM preparation, the vapor phase process is also promising particularly because it has no need for the use of a large amount of solvents which are necessary in the liquid phase processes. Furthermore, the deposition of aggregated organosilane molecules, which frequently degrades the quality of the SAMs, is expected to be smaller in the vapor phase method than in the liquid phase method, since such aggregated molecules have lower vapor pressure and are rarely vaporized. Thus, the vapor phase method is considered to be practically convenient.

Samples were cut from Si wafers were cleaned by a UV/ozone cleaning method. The cleaned sample surfaces became completely hydrophilic with their contact angle with water to be less than 5°. The sample surfaces were most likely terminated with OH groups. The cleaned samples were placed together with a glass cup filled with 0.3 cm³ organosilane liquid into a 150 cm³ Teflon™ container. The container was sealed with a cap and then heated to 100 or 150 °C. For the application in scanning probe lithography, two types of organosilane molecules were used as precursors. The first was hexamethyldisilazane [HMDS, (CH₃)₃Si-NH-Si(CH₃)₃, Fig. 1a] which has a vapor pressure of 79 Torr at 50 °C [14]. The second was octadecyltrimethoxy silane [OTMS, CH₃(CH₂)₁₇Si(OCH₃)₃, Fig. 1b] which has a vapor pressure of 2 Torr at 150 °C [14].

The organosilane molecules in the container vaporized and reacted with the surface OH sites on each sample. The molecules were chemisorbed onto the sample resulting in the formation of an organosilane monolayer. As illustrated in Fig. 1, a trimethylsilyl (TMS) monolayer which consists of 3 methyl groups and one Si atom is formed from HMDS, while an octadecylsilyl (ODS) monolayer having a long alkyl chain

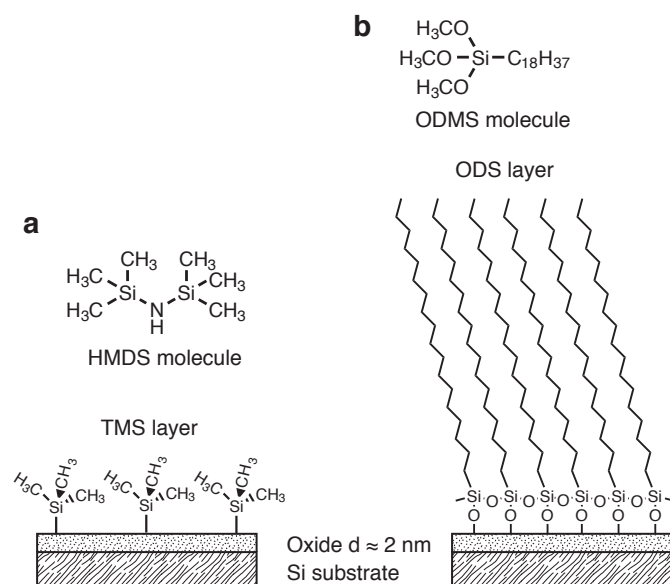


Figure 1. Chemical structures of (a) HMDS molecule and TMS monolayer, (b) OTMS molecule and ODS monolayer.

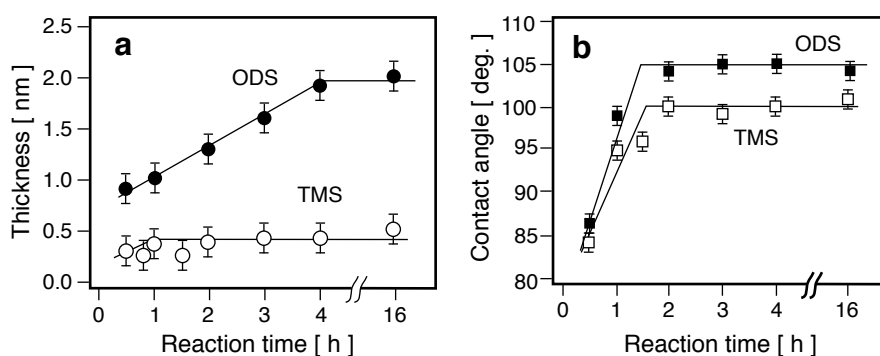


Figure 2. Rate of formation of organosilane monolayers. a) Thickness of the monolayers estimated by ellipsometry. b) Water contact angle of the monolayers.

of 18 carbons is formed from OTMS. The thickness of the monolayer was estimated by ellipsometry. Measurements were made using an ellipsometer (Nikon, NPDM-1000) with a 100 W halogen lamp as a light source. The light wavelength and the incidence angle for the measurements were set at 600 nm and 70°, respectively. We calculated each sample's monolayer thickness using 3.947-0.0257i as the refractive index of Si and assuming that the monolayer and the native oxide on the Si substrate were transparent at this wavelength and had the same refractive index of 1.46. Since the resulting value was the sum of the thicknesses of the monolayer and the native oxide, the actual monolayer thickness was determined by subtracting the oxide thickness from the total. Before monolayer coating, the thickness of the native oxide layer of each sample was measured. These were determined to be around 2 nm.

Figure 2 follows the formation of TMS and ODS monolayers by the vapor phase method at a temperature of 100 °C. After a reaction time of 2 hours, TMS and ODS monolayers both showed hydrophilicity with contact angles of ca. 100° and 105°, respectively, indicating that the substrate surfaces had become terminated with alkyl groups. In addition, the ODS monolayer showed a slightly larger contact angle than that of the TMS monolayer. These results agree with the reported dependence of water contact angle on the alkyl chain length of organosilane monolayers [11].

The thickness of the TMS monolayer was ca. 0.4 nm and, as seen in Fig. 2a, changed little during the period from 0.5 to 16 hours. This thickness data seems to indicate that monolayer formation was almost completed within 1 hour. Nevertheless, we concluded that at least 2 hours was necessary to completely form the TMS monolayer, since 2 hours was required for the contact angle of the TMS monolayer to reach its maximum. The thickness of the ODS monolayer reached a plateau of ca. 2 nm after 4 hours, as shown in Fig. 2a. The growth rate of the ODS monolayer was slower than that of the TMS monolayer because the vapor pressure of OTMS is lower than that of HMDS. It was concluded that ODS monolayer formation was complete after 4 hours, although the water contact angle of the ODS monolayer reached a saturated value of 105° after only 2 hours (Fig. 2b). The film thicknesses of the TMS and ODS monolayers prepared by the vapor phase method for 16 hours at 150 °C were the same as those of the monolayers prepared at 100 °C.

3. Patterning of organosilane SAMs by SPM

3-1. SPM patterning of organic thin films

The patterning of organic thin films is of special importance due to their application as lithographic resists. There have been numerous reports describing the SPM-based patterning of organic molecular films. For example, spin-coated polymer films and Langmuir-Blodgett films have been patterned using scanning tunneling microscopes (STMs) operated in vacuum [15-17] as well as by using STMs or atomic force microscopes (AFMs) operated in air [18,19]. SAMs have also attracted attention due to their excellent uniformity in molecular order. Organic thiol SAMs on gold or gallium arsenide substrates have been demonstrated as SPM-patternable films [20-22]. SAMs consisting of organosilane molecules show great potential as ultrathin resist films. An STM operated in a vacuum has been applied to the patterning of an organosilane SAM [23,24]. We have succeeded in fabricating nano-scale patterns on an alkylsilane monolayer on Si and a fluoroalkylsilane monolayer on Ti under an ambient atmosphere [25-29].

3-2. Scanning probe anodization

When an SPM is operated in a humid atmosphere, it is well known that a water column of nanometer in diameter is formed at the SPM-tip/sample junction as schematically illustrated in Fig. 3. When an appropriate bias voltage is applied to the junction, such a water nanocolumn work as a very minute electrochemical cell in which electrochemical reactions are induced in a spatially confined manner. These electrochemical reactions can be used for the localized surface modification at the SPM-tip/sample junction. In particular, the

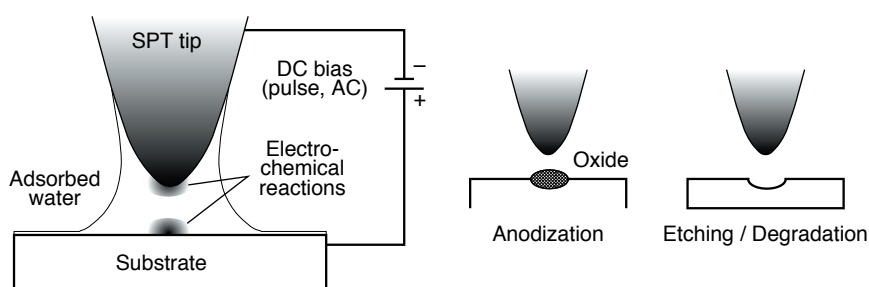


Figure 3. Schematic illustration of scanning probe anodization in a humid atmosphere.

junction bias is applied to be the sample being as anode, electrochemical oxidation reactions are induced on the sample surface. When the sample substrate consists of a material on which an oxide film can be formed by anodization, that is, electrochemical oxide formation, oxide nanopatterns can be drawn on the substrate. Indeed, in early 1990's, we and other research groups have demonstrated SPM-based surface oxidation, that is, scanning probe anodization, of metals and semiconductors [30-35]. An interesting phenomenon happens when graphite is used as a sample for scanning probe anodization. The carbon network in graphite is electrochemically decomposed. Consequently, the graphite surface is locally etched instead of forming oxide [38], following researches on local oxidation of hydrogen-terminated Si surfaces cathodically polarized beneath an STM tip [36,37]. If we employ an organic film as a sample for scanning probe anodization, it is expected that C-C chains of the organic film are degraded as well and the film is etched as similarly to graphite.

3-3. STM lithography

In this section, the SPM-lithography processes with the TMS monolayer (Fig.1a) based on using an STM is demonstrated [27,28]. The monolayer prepared on a Si substrate was locally degraded in a region where the STM tip had been scanned while positively (+5 ~ 10 V) biasing the substrate Si. The patterns on the degraded monolayer were transferred to the Si substrate by chemical etching using the degraded regions as etching windows. In addition, we studied how the atmospheric environment affected the tip-induced degradation of the TMS monolayer. The degradation rate was enhanced by an increase in humidity or O₂ concentration in the atmosphere.

The experiments were conducted using an STM (Seiko Instruments, SPI-3600) with a conductive diamond tip. The STM unit was set in a closed box with a volume of ca. 8500 cm³. STM-tip scanning on the samples was conducted in air or atmosphere purged with N₂ or O₂ gas flow for at least 2 hours. Relative humidity (RH) was reached an equilibrium of about 20% or 5% during gas purge at a flow rate of 200 or 1000 cm³/min, respectively.

A Si surface covered with a TMS layer (TMS-Si) was first scanned in air with an arbitrary pattern by the STM at a sample bias (Vs) of +5.0 V, a reference current (i) of 0.2 nA and a tip-scanning speed (v) of 0.6 μm/sec. This sample was then immersed in a 30wt.% H₂O₂ aqueous solution for 5 min. As shown in Fig. 4a, the condensation of the atmospheric water on the sample surface was observed by optical microscopy. An optical microscope, Nikon, Optiphot-2, with a differential interference contrast (DIC) attachment was used. The micrograph clearly indicates that the regions where the tip-scanning took place have become hydrophilic, while the surrounding area has remained hydrophobic. It is plausible that the methyl (CH₃) groups of the TMS layer were replaced with OH groups as a result of the STM-tip scanning. Namely, the TMS monolayer had been removed and, consequently, the underlying SiO₂ surface was exposed. The H₂O₂ treatment was not absolutely necessary for the water condensation, however, it seemed to improve the hydrophilicity of the degraded regions. It should be noted that we could not locate the scanned regions by DIC microscopy without the water-condensation. However, it can be imaged using an AFM that the tip-scanned region was slightly protruded (< 1 nm) from the surrounding undegraded area as shown in Fig. 4b. This is most certainly due to volume expansion resulting from the anodization of the substrate Si which immediately followed the STM-tip induced degradation of the TMS layer.

Some of the patterned samples were etched in a solution of ammonium fluoride (NH₄F): H₂O₂: H₂O =

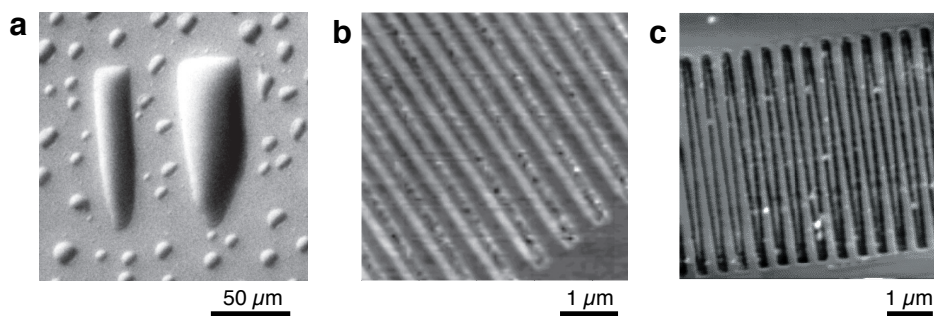


Figure 4. STM lithography. a) Optical micrograph of atmospheric water vapor condensed onto the patterned Si-TMS surface. STM patterning was conducted with Vs = +5.0 V, i = 0.2 nA and v = 0.6 μm/s in air. b) AFM image of a line pattern fabricated on a TMS-Si sample. The lines were generated by STM patterning with Vs = +5.0 V, i = 0.2 nA and v = 1.2 μm/s in N₂ with 20%. c) AFM image of a Si nanostructure fabricated through the STM lithography and chemical etching.

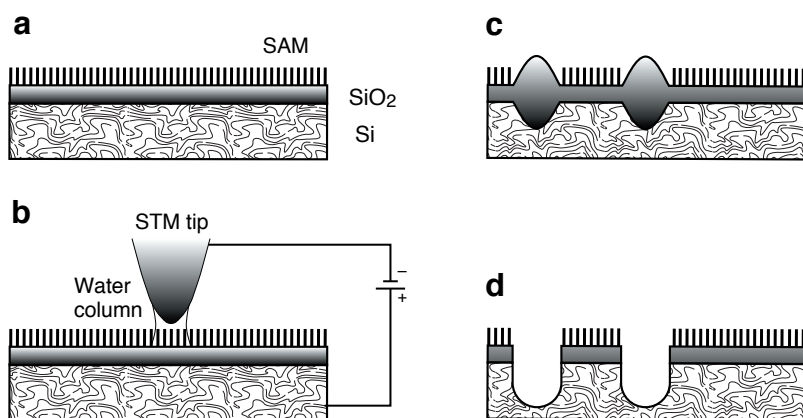


Figure 5. Schematic diagram of STM lithography. a) Preparation of a TMS monolayer on Si substrates (TMS-Si). b) STM Patterning. c) Patterned sample. d) Pattern transfer to the Si substrate by chemical etching.

10 g : 3 g : 100 g at room temperature. Figure 4c shows an etched Si structure patterned by the STM. The etching was prolonged for 5 min after the patterning. The scanned region was selectively etched, while the unscanned region was protected from etching by the undegraded TMS monolayer. As can be seen in the AFM image, fine grooves as narrow as 60 nm were fabricated. The grooves were 10 nm deep.

This STM lithography process is summarized in Fig. 5. In the first step (Fig. 5a), a TMS monolayer was prepared on an oxide-covered Si substrates. Then, in the next step (Figs. 5b and 5c), the samples were patterned by STM similarly to scanning probe anodization. In the final step (Fig. 5d), the patterned samples are chemically etched. Since both Si and SiO_x dissolves in the $\text{NH}_4\text{F}/\text{H}_2\text{O}_2/\text{H}_2\text{O}$ etching solution while the TMS monolayer is relatively resistant to etching, the substrate is etched through the etching window created by the degraded TMS monolayer. The etching of the substrate in the solution proceeds isotropically such that the etched groove widens due to side-etching as etching time increases. The process shown here requires no further step of resist development; therefore the TMS monolayer can be regarded as a self-developing SPM resist. Patterning and developing occur simultaneously during probe scanning.

The spatial resolution of scanning probe lithography is primarily governed by the tip shape and its scanning direction. In the present experiment, the degradation of the TMS monolayer, and therefore the STM lithography, are affected by the tip shape. The AFM image in Fig. 6 demonstrates this tip-shape effect. It is clear that the STM tip used for this experiment had dual peaks which resulted in the formation of double parallel lines, one 90 nm wide and 20 nm deep and the other 60 nm wide and 12 nm deep. When the tip-scan direction was turned perpendicular, these lines overlapped and formed a single line groove 120 nm wide and 20 nm deep.

The effects of atmosphere on the tip-induced degradation of the TMS monolayer were studied in detail through AFM observation of etched samples. A TMS-Si sample was patterned three times by STM. Each

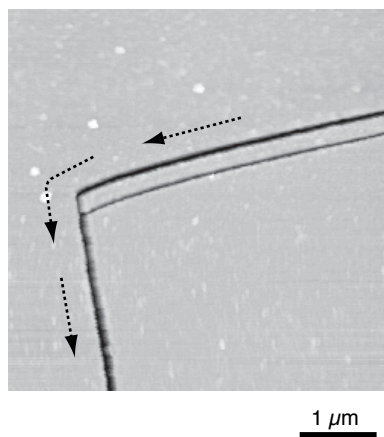


Figure 6. AFM image of grooves fabricated on a Si substrate using a dual-peaked STM tip. The TMS-Si sample was etched for 5 min after being scanned by the STM ($V_s = +5.0$ V, $i = 0.2$ nA and $v = 1.2$ $\mu\text{m}/\text{sec}$) in N_2 with 80%RH.

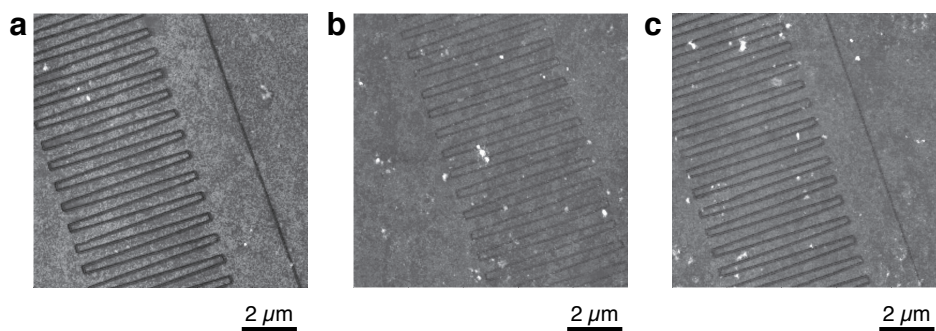


Figure 7. AFM image of etched grooves on a Si substrate showing the dependence of the STM-tip-induced degradation ($V_s = +5.0$ V, $i = 0.2$ nA and $v = 0.7$ $\mu\text{m}/\text{sec}$) of the TMS monolayer on atmosphere. a) Low-humidity N_2 (5%RH), b) high-humidity N_2 (80%RH), and (c) low-humidity O_2/N_2 (20 $\text{O}_2\text{vol}\%$, 5%RH).

patterning was performed in a different type of atmosphere: first, in a low humidity (5%RH) N_2 atmosphere; second, in a high humidity (80%RH) N_2 atmosphere; and finally, in a O_2/N_2 (20vol.% O_2) atmosphere with a low humidity (5%RH). The sample was etched for 5 min, and then observed by AFM. Results are shown in Figs. 7a, 7b and 7c. The groove fabricated after the STM patterning in the low-humidity N_2 atmosphere (Fig. 7a) is fainter than that fabricated after patterning in the high-humidity N_2 atmosphere (Fig. 7b). The groove depths, estimated from these AFM images, are about 5 and 10 nm, respectively. It is clearly indicated that the degradation of the TMS monolayer proceeded more efficiently under the high-humidity condition. In contrast, under low-humidity conditions, the TMS monolayer degraded less due to the shortage of chemical species, i.e., adsorbed water, required for the electrochemical reactions. This less-degraded region showed some resistivity to the etching and, accordingly, the etch depth became shallow compared with that in the well-degraded region prepared under the high humidity condition. It is noteworthy that, when etching was conducted for 3 min, the etched depth in the region degraded under the low humidity condition was very shallow, only 1 nm or less, while the region degraded under the high humidity condition was already clearly etched. Furthermore, when the degraded lines were relatively wide due to the use of a blunt tip for patterning as, for example, in Fig. 7a, the etching did not proceed uniformly over the entire line area, with the result that the etched structures did not form complete grooves when the etching time was insufficient. Under such a low humidity condition, the degradation rate is determined by the amount of adsorbed water at the tip-sample junction supplied from the atmosphere. These results are definite evidence that the degradation mechanism is primarily governed by electrochemical reactions involving adsorbed water. The image shown in Fig. 7c demonstrates the effect of oxygen on the monolayer degradation. The depth of the groove fabricated after STM patterning in the atmosphere containing O_2 is estimated to be about 7 nm, based on the AFM image. It is slightly deeper than that fabricated under the same low-humidity condition without O_2 (~ 5 nm, Fig. 7a). O_2 participated in the degradation reaction and enhanced its rate probably through dissolving into the adsorbed water, similarly to the scanning probe anodization of Ti [33].

The area of scanning probe anodization, namely, its spatial resolution, was reported to increase under high-humidity conditions [33]. However, as shown by the AFM images in Fig. 7, the groove widths are almost the same regardless of humidity. The width was estimated to be about 90 nm from magnified AFM images. We also confirmed that both the width and depth of the etched grooves slightly increased with humidity when a sharp tip was used for the patterning. However, we have not yet identified whether this groove broadening was due to enlargement of the reaction area or to side etching. Nevertheless, these experimental results imply that the area of the tip-induced electrochemical reaction was primarily determined by the tip's shape and was less dependent on humidity, in contrast to the results for the scanning probe anodization of Ti. This result can be explained with the hydrophobic nature of the TMS monolayer. Under a high-humidity condition, a thick water layer is adsorbed onto a Ti surface, since it is hydrophilic due to the presence of native oxide. The lateral diffusion of ionic species carrying faradaic current is significant under such conditions. Consequently, the Ti surface becomes anodized over a large area up to a few micrometer in diameter beyond that which is beneath a tip. In contrast, the TMS monolayer surface is very hydrophobic so that the amount of adsorbed water is small even under high humidity condition. It has been reported that the amount of adsorbed water on a TMS monolayer was one-sixth of that on a hydrophilic silica surface at 80%RH [39]. Thus in the case of the TMS monolayer, the electrochemical reactions are primarily governed by the adsorbed water on the tip and, consequently, are less dependent on humidity than in the case of Ti

anodization.

3-4. AFM lithography

Among various types of scanning probe lithography, that based on AFM is particularly promising, since this technique provides us with versatility in patterning materials and with high patterning speed in the range of hundreds ~ thousands of $\mu\text{m}/\text{sec}$ as described in this section and other papers [40-43]. Other important advantages of the AFM-based scanning probe lithography are compatibility with a high throughput lithography such as photolithography [44-47] and that with in-situ electrical characterization of fabricated nanopatterns [48,49].

The AFM lithography process as shown in Fig. 8 is similar to that of the STM lithography except the patterning step. In the AFM lithography, the samples were patterned using an AFM with a conductive probe. Use of AFM for the patterning instead of STM has the advantage that the probe position can be controlled independently of modification mechanisms, in the present case, junction current.

3-4-1. AFM lithography with TMS monolayer resist

We have studied the bias dependence of the TMS monolayer degradation using an AFM (Park Scientific Instruments, Autoprobe-CP) with a conductive probe (a custom made microfabricated silicon nitride probe coated with a 20-nm-thick NiCr layer, force constant = 0.4 N/m). A source measure unit (SMU Model 236, Keithley) was installed in this AFM to apply a bias voltage between the sample and the probe and to measure current during patterning. A sample was patterned at various sample bias voltages (Vs). The probe scanning was conducted in $5 \mu\text{m}$ -square regions with 256 lines at a scanning speed (v) of $10 \mu\text{m}/\text{sec}$ in air at 60%RH. Throughout this experiment, the same probe was used with an identical setting force (about 10 nN) in order to minimize any variation in contact area and its subsequent effect. After the patterning, the sample was etched in a solution ($\text{NH}_4\text{F} : \text{H}_2\text{O}_2 : \text{H}_2\text{O} = 10\text{g} : 3\text{g} : 100\text{g}$) and then observed by AFM.

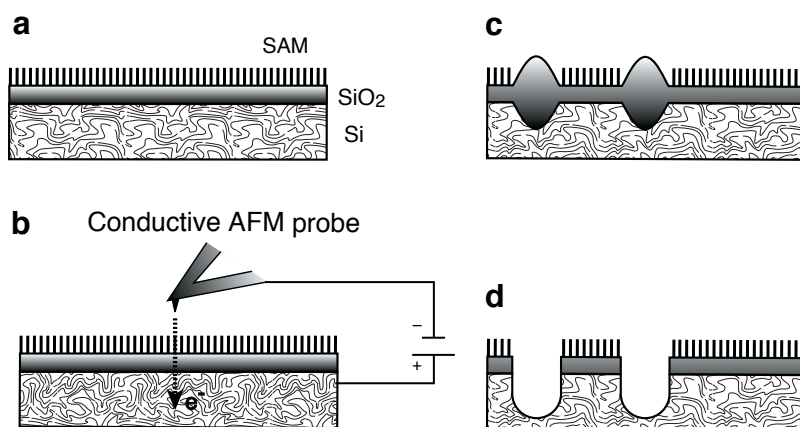


Figure 8. Schematic diagram of AFM lithography. a) Preparation of an organosilane monolayer on Si substrates (TMS-Si, ODS-Si). b) Conductive AFM Patterning. c) Patterned sample. d) Pattern transfer to the Si substrate by chemical etching.

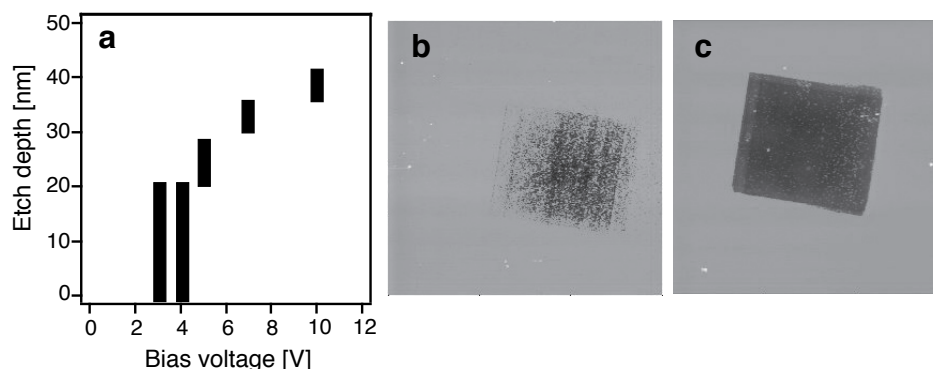


Figure 9. Bias dependency on the AFM lithography for nanostructuring of the TMS-Si samples. a) Depth of the etched regions. AFM images of etched structures patterned at Vs = (b) +3.0 (b) and (c) +7.0 V.

When the substrate Si was polarized positively, the current (i) during the probe-scanning increased with V_s . The average i values were 10, 20, 30, 50, 60 and 100 pA at $V_s = +2.0, +3.0, +4.0, +5.0, +7.0$ and $+10.0$ V, respectively. The measured i values fluctuated almost 30 % from these averages. Figure 9a shows the etch depths plotted against the absolute voltage of V_s . At $V_s \geq +3.0$ V, depressed features appeared after the etching, while, at $V_s = +2.0$ V, there were no etched features observable by AFM. At $V_s = +3.0$ and $+4.0$ V, the etch depths are shown as long bars since the etching did not proceed uniformly in the scanned region and unetched parts remained. The depth of the etched parts was about 20 nm. The area of the etched part was larger at $V_s = +4.0$ V than at $V_s = +3.0$ V. At $V_s \geq +5.0$ V, the entire scanned area became etched. The depths of the etched regions were 25, 33 and 40 nm at $V_s = +5.0, +7.0$ and $+10.0$ V, respectively. The results at $V_s = +3.0$ and $+7.0$ V are shown in Fig. 9b and 9c as examples.

The substrate etching begins in the regions where the TMS monolayer has been degraded to some extent and then proceeds isotropically, i.e., both laterally and vertically. Therefore, the substrate is etched more deeply and broadly with an increase in the degree of monolayer degradation in a scanned area. The results shown in Fig. 9 demonstrate that the degradation rate increased with V_s . At $V_s = +2.0$ V, the rate was so low that the etching apparently did not proceed.

In Section 3-3, we described that the degradation of the TMS monolayer induced by an STM-tip could be conducted even in a nitrogen atmosphere if humidity was appropriate, and furthermore, that the degradation rate accelerated with an increase in humidity. We have also confirmed that the voltages corresponding to onset of the TMS monolayer degradation (to be referred to as V_{onset} at which the substrate etching apparently began), increased under low humidity conditions. For example, in air with 10 ~ 20%RH, V_{onset} was $+5.0 \sim +6.0$ V. This is further proof that the degradation is primarily governed by electrochemical reactions with adsorbed water.

3-4-2. AFM lithography with ODS monolayer resist

In this section, we report on surface modification of the ODS monolayer on Si (ODS-Si) by injecting current from an electrically conductive AFM probe. The advantage of the ODS-monolayer over the TMS-monolayer is its thickness. Since, the ODS-monolayer consists of alkylchains with 18 carbons, the monolayer more effectively shields its substrate from an environment. Namely, the ODS monolayer is more stable chemically than the TMS-monolayer and is favorable for pattern transfer processes such as chemical etching.

The ODS monolayer was modified using an AFM (Seiko Instruments Inc., SPA-300HV+SPI-3800N). In order to inject current into the ODS-Si sample, a DC bias voltage was applied between the conductive AFM probe and the substrate Si which served as cathode and anode, respectively. An electrically conductive probe (Park Scientific Instruments, Ultralever, a heavily doped Si probe) was used. The probe was normally pressed to the sample surface at a load force of ca. 3 nN. Topographic and lateral force microscope (LFM) images of the surface-modified ODS-Si samples were acquired using the same AFM used for patterning.

Figure 10a shows an LFM image of a patterned ODS-Si sample surface. The square feature showing a higher lateral force corresponds to the region at where current was injected from an AFM probe while scanning at $v = 0.1 \mu\text{m}/\text{sec}$. The probe was pressed to the sample surface at a load force of 2.8 nN. A bias voltage of 10 V was applied between the probe and the substrate Si. From a topographic AFM image of this sample, the probe-scanned region was confirmed to protrude a few nanometers from the surrounding ODS-Si surface where current was not injected at all. On the contrary, there are no features detectable by LFM on the ODS-Si sample scanned and current-injected in vacuum at a pressure of 1.5×10^{-6} Torr, although the

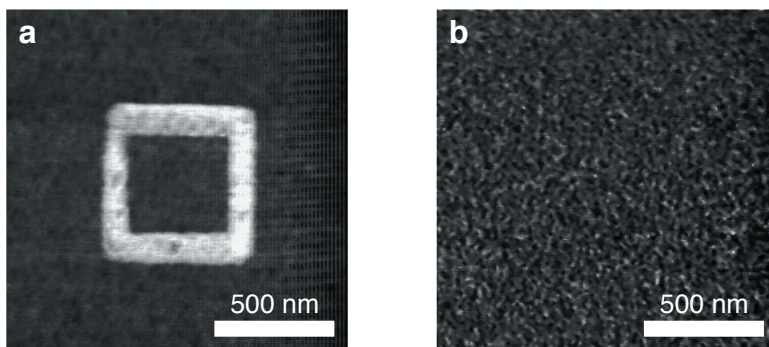


Figure 10. LFM images of the ODS-Si sample surface processed by the AFM lithography. Prior to imaging, both the surfaces were scanned with an AFM probe along a $1\text{-}\mu\text{m}$ square pattern while injecting current. Patterned scanning was conducted in air (a) or in vacuum (b).

same bias and load force were applied as well. Mechanical scratching is not a mechanism of the surface modification as shown in Fig. 10a, since the ODS-Si is so robust that no damages were induced even at a load force of 600 nN [50]. The surface modification of ODS-Si progresses when current is injected in air as demonstrated in Fig. 10a. We, thus, conclude that the ODS-Si sample was modified through electrochemical reactions proceeding in the adsorbed water column formed at the probe-sample junction as similarly to scanning probe anodization. Due to these reactions, the organic molecules consisting of the ODS monolayer were anodically degraded and finally decomposed. Consequently, a lateral force contrast between the modified and unmodified regions was generated. In addition, anodization of the substrate Si occurred simultaneously so that the current-injected region protruded [23-26].

Dot features were fabricated on another ODS-Si sample by placing an AFM probe at each of the positions and applying a bias voltage from 0.01 to 50 seconds. As clearly seen in lateral force and topographic images (Figs. 11a and 11b, respectively), dimensions of these dot features depend on the bias duration time. Lateral and vertical dimensions of the dot features estimated from lateral force and topographic images are summarized in Figs. 12a and 12b, respectively. At $V_s < +4.0$ V, we could not find any fabricated features. This threshold voltage is higher than that in AFM lithography of the TMS monolayer. Since the ODS-monolayer is more electrically insulative than the TMS monolayer due to the greater thickness of the ODS-monolayer. Accordingly, a higher bias voltage is needed to inject current to the ODS-monolayer.

The dot features grow both in the lateral and vertical directions with the increases in duration time and bias voltage. The growth in height of the dot features are summarized with the bias voltage as shown in Fig. 12a. Chemical properties of the modified surfaces are studied by comparing lateral force contrasts between the modified and unmodified ODS-Si surfaces. The results are summarized in Fig. 12b. At $V_s \geq +5.0$ V, lateral force contrast increases with an increase in bias duration time. However, it seems to be constant around 100 - 140 mV at certain duration times dependent on V_s . For example, at $V_s = +10.0$ V, lateral force contrast becomes constant when the bias is applied for more than 0.5 seconds, while, duration times longer than 1 second are needed at $V_s = +7.0$ V. However, at $V_s = +4.0$ V, lateral force contrast never reaches to

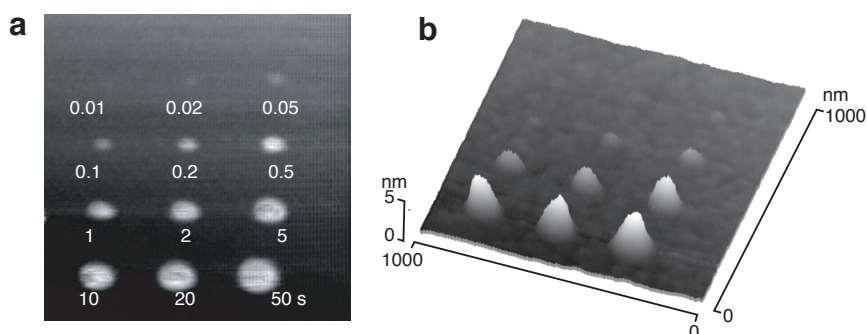


Figure 11. Lateral force (a) and topographic (b) images of dot features fabricated on an ODS-Si sample. A bias (+10 V) duration time for each of the dot features are indicated in the LFM image.

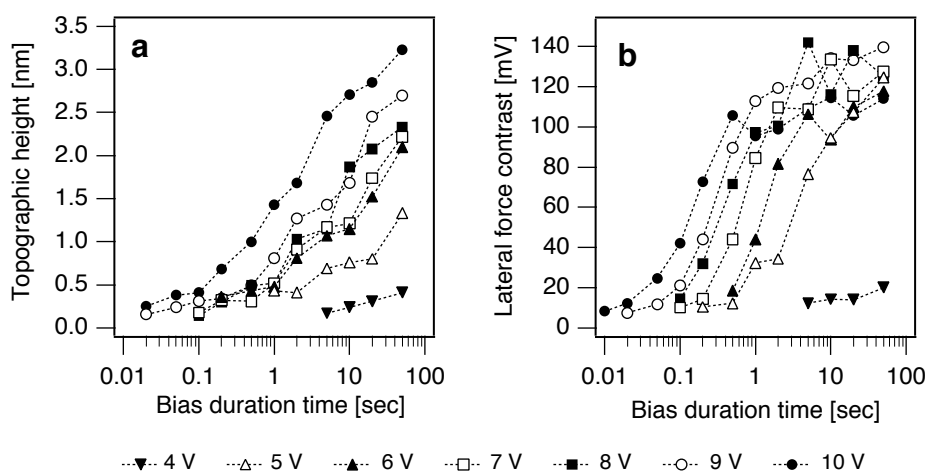


Figure 12. Dot height (a) and lateral force contrast (b) vs. bias duration time.

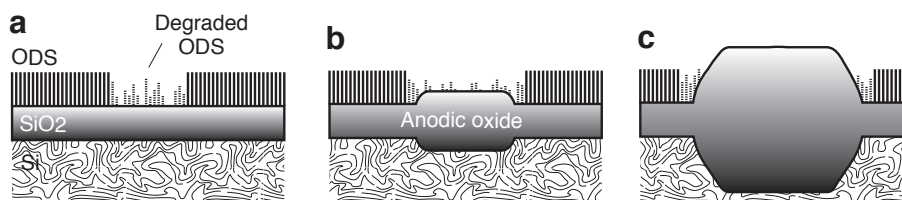


Figure 13. Schematic illustration of initial (a), middle (b) and final (c) stages for the surface modification of ODS-Si induced beneath the AFM probe.

the constant value. The bias voltage of 4 V is not sufficient in order to complete the surface modification of the ODS monolayer. In addition, it is noteworthy that, when we compare the lateral force contrast and topographic height, for example, of the dot features fabricated at $V_s = 10$ V, the topographic height is found to still increase even after the lateral force contrast becomes constant (bias duration time > 0.5 sec).

From these experimental results, we discuss the surface modification processes progressed at the probe/sample junction as follows. At the initial stage, the organic molecules are chemically modified, decomposed and probably removed in a part of the probe scanned region. Consequently, the underlying oxide surface partly appears as illustrated in Fig. 13a. Since surface of silicon oxide has a frictional coefficient larger than that of ODS-Si and the capillary force effect on such a hydrophilic oxide surface is larger than that on the hydrophobic organic monolayer surface [51], the lateral force contrast between the modified and unmodified regions is generated. When the surface modification is further progressed, anodization of the substrate Si begins. This is probably because ions necessary for the anodization become to move through the degraded ODS-SAM. However, some parts of the organic monolayer still remain on the surface as shown in Fig. 13b. In the final stage (Fig. 13c), the organic molecules have been decomposed completely and, only the Si anodization further proceeds in this stage. Therefore, lateral force contrast does not change since the modified surface consists of silicon oxide throughout the final stage, although it protrudes due to the progress of the Si anodization.

Besides dot structures, lines were drawn as shown in an LFM image of Fig. 14a. Line widths, estimated from LFM images, are summarized in Fig. 14b. As expected, the line width decreases when the probe scanning speed becomes faster. When V_s is reduced, thinner lines can be drawn at the same scanning speeds. However, in the scanning speed region faster than $0.1 \mu\text{m}/\text{sec}$, the line width is seems to be minimum at around 20 nm, independently of V_s and probe scanning speed. This limitation in line width is most likely due to the actual probe size used for the patterning.

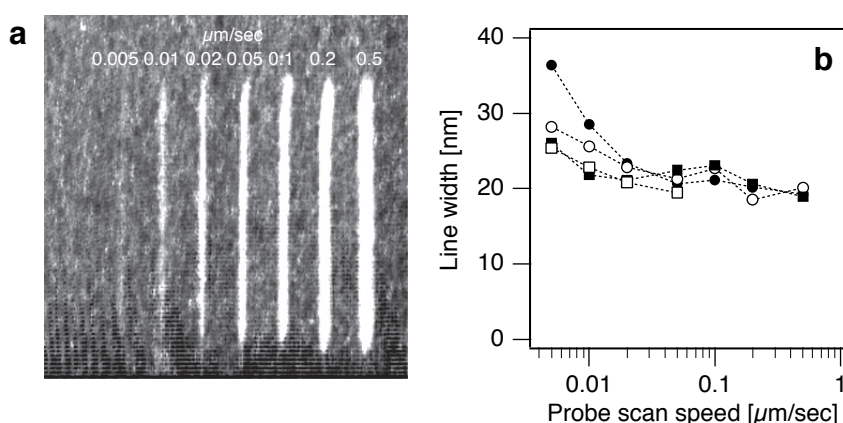


Figure 14. Line pattern drawing on an ODS-Si sample by AFM lithography. a) LFM image ($1 \mu\text{m} \times 1 \mu\text{m}$) of the lines drawn at $V_s = 10$ V. b) Width of the line patterns at various probe scan speeds.

4. Advanced probe lithography

4-1. Constant-current AFM lithography

Figure 15 shows AFM images of grooved structures fabricated on a TMS-Si sample by patterning in air with 60%RH at $V_s = +10.0$ V with various v values by the $\text{NH}_4\text{F}/\text{H}_2\text{O}_2/\text{H}_2\text{O}$ chemical etching for 3 min. The

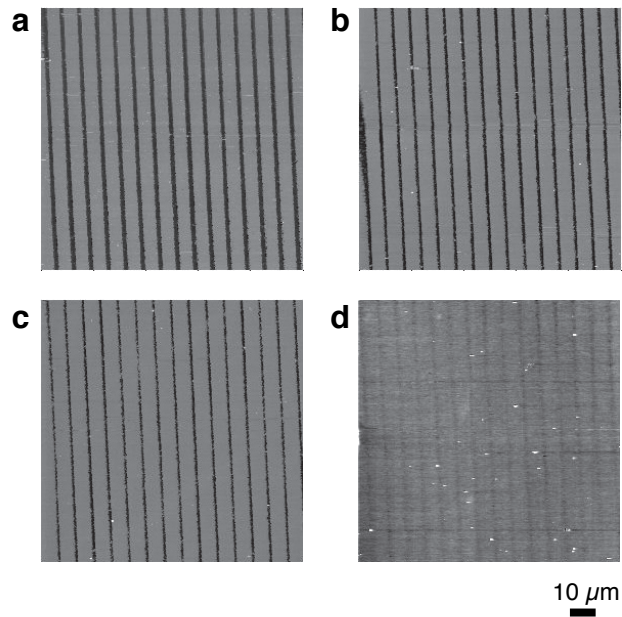


Figure 15. AFM images of etched grooves on a TMS-Si sample showing the dependence of the AFM-induced degradation rate on probe scan rate. (a) 20, (b) 80, (c) 160 and (d) 400 $\mu\text{m}/\text{sec}$. The size of each image is 10 $\mu\text{m} \times 10 \mu\text{m}$.

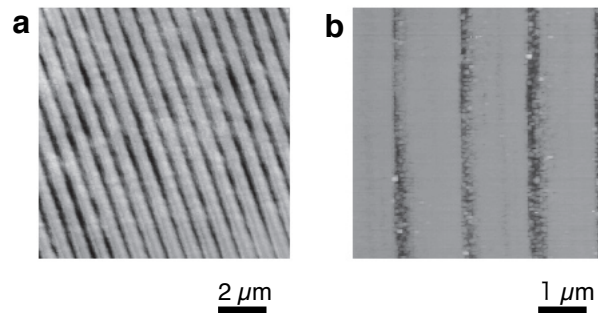


Figure 16. AFM images of etched grooves on a Si substrate demonstrating the constant current AFM-lithography at a patterning speed in the order of thousands of $\mu\text{m}/\text{sec}$, i. e., $v =$ (a) 1000 and (b) 5000 $\mu\text{m}/\text{sec}$. Patterning was conducted in air with 40%RH using a Si probe at line dose rates = 5 and 4 $\text{pC}/\mu\text{m}$, respectively. Etching time was 6 min for sample (a) and 3 min for sample (b).

etched depth increased with an increase in v . The estimated values were 27 ~ 30, 18 ~ 20 and 14 ~ 16 nm at $v = 20, 80$ and 160 $\mu\text{m}/\text{sec}$, respectively. Line dose rates for these patterning were estimated to be 5, 1.3 and 0.63 $\text{pC}/\mu\text{m}$, respectively, from an average current of 0.1 nA during patterning. Groove width increased with v decrease due to increased side-etching effect as can be seen in Fig. 15. The degree of monolayer degradation depends on v , therefore, the amount of injected current per unit area. At $v = 400 \mu\text{m}/\text{sec}$ (Fig. 15d), the groove depth, probably less than a few nm, was too shallow to be determined precisely due to the friction effect on AFM. The degree of the degradation was insufficient at this probe scan rate with a line dose rate of 0.25 $\text{pC}/\mu\text{m}$. For TMS resist, a line dose around 1 $\text{pC}/\mu\text{m}$ or higher is necessary to draw clear patterns.

By applying a higher bias voltage, we can increase injecting current and, consequently, degrade the monolayer sufficiently even at a high scan speed. However, the controllability of the current was not satisfactory in using the constant bias mode AFM lithography, different from the STM lithography in which both bias and current are controllable to be constant. The relationship between the junction current and the bias voltage depends on several factors, such as the age and idiosyncrasies of the particular probe used. The current could not be precisely controlled by simply applying a defined bias voltage. In order to overcome this shortcomings, we have developed and reported for the first time the constant current mode AFM lithography [42]. In this experiment, an AFM (Park Scientific Instruments, Autoprobe-CP) was used with a conductive Si probe. The constant current source in the SMU installed in the AFM was used in order to control the electric current flowing through the junction of the AFM-probe and the sample.

As demonstrated in Fig. 16, by controlling the junction current in order to attain a line dose in the range of several $\text{pC}/\mu\text{m}$, we were able to fabricate clear etched structures even at line drawing speeds of $1000 \mu\text{m}/\text{sec}$ and above.

4-2. Multilayer resist for AFM lithography

In this section, we demonstrate the capability of the current-injecting AFM lithography for nanoprocessing of insulator [52]. We fabricated nanostructures of SiO_2 , which is a key insulating material for Si-based microdevices, based on the lithography. However, the AFM lithography cannot be directly applicable to patterning of insulating substrates, since the AFM lithography is based on the current flowing at the probe/sample junction. Therefore, we have developed a multilayer resist film combined the SAM and an electrically conductive film. Before selecting the conductive film, we considered the following conditions. First, it can be covered with an organosilane SAM. Second, it can be used as a mask for chemical etching of SiO_2 . Third, it can be formed as a thin and uniform film of a few tens of nm in thickness. Finally, it would be trouble-less and compatible to the fabrication process of Si-based microelectronic devices. Accordingly, amorphous silicon (a-Si) was chosen as a candidate and a multilayered resist film was prepared. In this resist system, the organosilane SAM and the a-Si films were served as an imaging layer and a current-passing layer, respectively.

Figure 17 shows a process chart of the AFM-lithography for SiO_2 nanopatterning using the multilayered resist film. A sample substrate was a single crystal Si plate with a thermally grown oxide layer of ca. 20 nm in thickness. A triple-layered resist film was prepared on this Si substrate (Fig. 17a). A thin Si film of 20 nm in thickness, which was confirmed to be amorphous by electron microscopy and diffractometry, was deposited on the substrate by ion-beam sputtering. Next, the sample was cleaned by a UV/ozone method. By this cleaning, organic contamination on the a-Si layer was removed and a clean surface oxide was photochemically prepared on the layer. The oxide surface was hydroxylated and, therefore, completely hydrophilic with its water contact angle less than 5° . Finally, an ODS monolayer was formed by the vapor phase method described in Section 2. Note that our multilayered resist film consists of triple layers, that is,

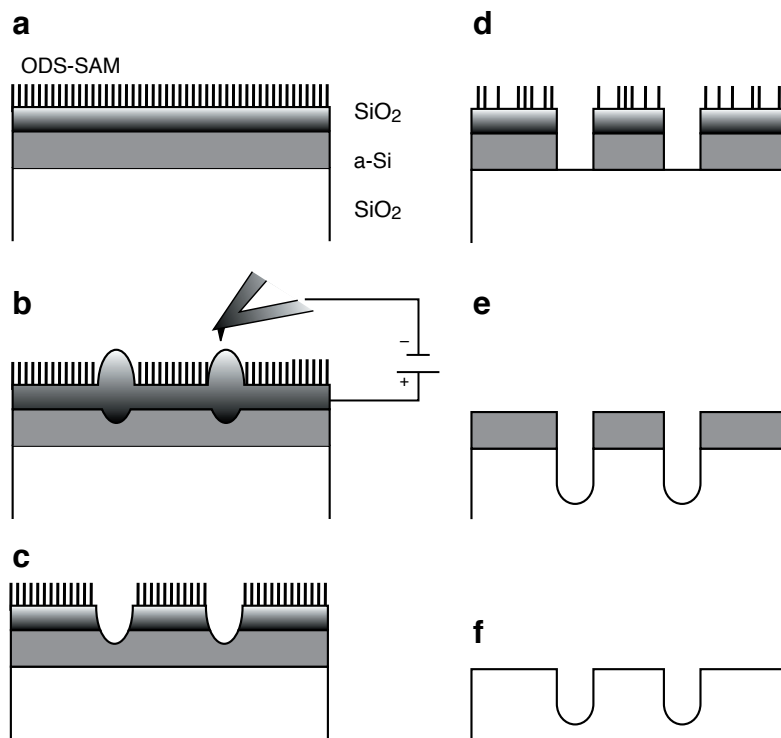


Figure 17. Schematic illustration of AFM lithography for nanopatterning of SiO_2 using the multilayered resist system. a) Cross section of a sample coated with a resist film. b) Resist exposure. Drawing patterns into the imaging layer (ODS monolayer) by current injection from a AFM-probe in constant current mode. c) Resist development Step I. HF-etching in order to remove the SiO_2 layer of the resist in the exposed area. d) Resist development Step II. TMAH-etching in order to remove the a-Si layer in the exposed area. e) Pattern transfer. HF-etching in order to remove the thermal SiO_2 in the exposed area. f) Resist removal. TMAH-etching for the whole a-Si layer.

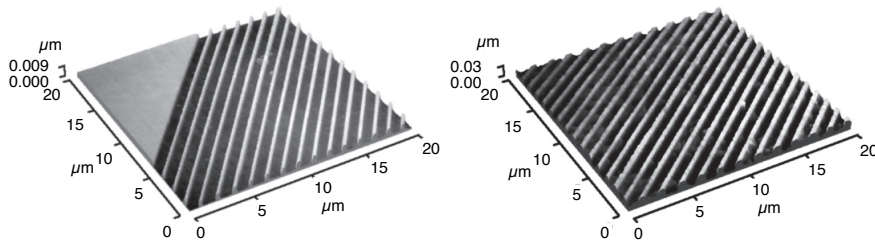


Figure 18. AFM patterning of a resist at a probe scan speed of 10 $\mu\text{m}/\text{sec}$ and a probe current of 5 nA. a) AFM image acquired after development Step I. b) AFM image acquired after development step II. The etching duration times were 0.5 and 3 min, respectively.

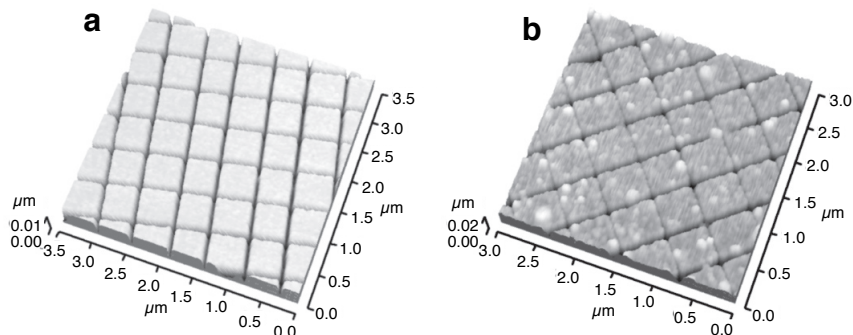


Figure 19. AFM images of a nanopatterned SiO_2 surface. AFM patterning was conducted at a probe scan speed of 20 $\mu\text{m}/\text{sec}$ and a probe current of 1 nA. a) AFM image of the exposed and developed resist film through Steps I and II prolonged for 0.5 and 3 min, respectively. b) AFM image of the SiO_2 substrate etched for 5 min in HF using the developed resist as an etching mask. The etch depth was estimated to be ca. 10 nm. Prior to imaging, the resist film was removed by TMAH etching for 4 min.

the ODS monolayer, the photochemically grown SiO_2 layer and the a-Si film from the top surface of the resist. This intermediate SiO_2 layer is crucial for this resist system, since, without this, the SAM is not formed. The SAM formation proceeds due to the chemical reaction between precursor organosilane molecules and OH sites on the oxide surface.

The sample was patterned using an AFM (Park Scientific Instruments, Autoprobe-LS) as shown in Fig. 17b. In order to inject current into the ODS monolayer, a bias voltage was applied between the conductive AFM probe (Park Scientific Instruments, Ultralever, a heavily doped Si probe) and the a-Si layer of the resist which was positively polarized. The patterning was conducted by the constant current mode using the SMU.

The developing process for the exposed resist film was a two-step chemical etching conducted at room temperature. Here we demonstrate this resist development using rather wide lines that were drawn by the use of a blunt tip probe for ease of etch depth measurement. At the first step of the process (Step I, Fig. 17c), the exposed resist film was etched in an aqueous solution of 0.5 wt.% hydrofluoric acid (HF). Figure 18a shows an AFM image of the resist film after Step I. In the current injected region, i.e., where the probe had been passed, both the photochemical and anodic oxides selectively etched while the unscanned region remained unetched due to the protection by the ODS monolayer. The etch depth, estimated to be ca. 5 nm from the cross section of the AFM image, was slightly greater than the sum of the thicknesses of the ODS monolayer and the photochemical oxide, that is, 4 nm at the thickest. This result indicates that the bottom a-Si layer was also etched to the depth of at least 1 nm and, thus, had further oxidized due to anodization in the probe scanned region. Although organosilane SAMs are gradually degraded in HF solution, we confirmed that the ODS monolayer on Si endured at least for 5 min in 0.5wt.% HF solution.

At the second step of the resist developing process (Step II, Fig. 17d), the HF-etched resist was further treated in an aqueous solution of 25wt.% tetramethylammonium hydroxide (TMAH). Since, in this solution, Si is effectively dissolved while SiO_2 is rarely etched, the a-Si is expected to be locally etched in the region where its surface oxide had been removed. In addition, this a-Si etching actually stops when the whole a-Si layer is etched and the underlying substrate, i.e., thermal SiO_2 , is exposed. As clearly seen in the AFM image shown in Fig. 18b, the current-injected region became further etched compared with Fig. 18a. Its

depth was almost equal to the thickness of the a-Si layer in the multilayered resist. The probe scanning pattern printed in the imaging layer, that is, ODS monolayer, on top of the resist was successfully transferred into the a-Si layer. Thus, the developing process of the exposed multilayer resist was concluded to be completed. Note that the ODS monolayer is degraded during the TMAH etching, since Si-O-Si bondings which connect the monolayer and the SiO₂ layer are not sufficiently resistive to the alkaline solution.

Nanostructures were fabricated on the substrate SiO₂ through chemical etching using the developed resist film as an etching mask. Figure 19a shows an AFM image of a developed resist film with a grid pattern at horizontal and vertical intervals of ca. 500 nm. This sample was further etched in the HF solution. The grid pattern on the resist film was thus transferred to the thermal SiO₂ (Fig. 17e). degraded and did not sufficiently protect the oxide layer. After this pattern transfer step had been completed, the resist film was etched again in the TMAH solution. The remained a-Si layer was etched and degraded and removed from the sample (Fig. 17f). The result is shown in Fig. 19b. This AFM image demonstrates that fine grooves less than 50 nm in width were successfully fabricated on the thermal SiO₂ substrate, although some part of the a-Si film, i.e., particulate features seen on the surface remained after the final TMAH etching.

Pattern widening must occur during the pattern transfer processes since wet chemical etchings employed in the present experiments proceed isotropically. It becomes more significant when an etch depth increases. The minimum line width which can be written into the multilayer resist is thus determined by the most thick layer, that is, the a-Si layer. The resolution limit is thought to be larger than its thickness of 20 nm in the present case.

4-3. Integrated lithography

Although, scanning probe lithography is a powerful technique for nanofabrication, its patterning speed is relatively slow compared with that of electron beam lithography even though scanning probe lithography has attained patterning in the drawing speed range of mm/sec or higher. This is a serious disadvantage in practical application. One approach to improving the total throughput of scanning probe lithography is to complement this slow but high resolution lithography with a high speed, low resolution pattern transfer technique. The integration of photolithography and scanning probe lithography is the most promising way. In order to perform such an integration in practical, two key technologies are needed to be developed. The first one is a resist material which is commonly usable in both photo and scanning probe lithographies. The second one is an accurate alignment of an AFM-generated pattern with a photolithographically transferred pattern on the resist.

In this section, we report on the integration of scanning probe lithography with photolithography using organosilane SAM as a resist material both for scanning probe lithography and photolithography [47,53]. The process of this integrated lithography is explained using a process chart as schematically depicted in Fig. 20. In the first step of this integrated lithography, a monolayer resist is patterned by vacuum ultraviolet (VUV) light irradiation through a photomask (Fig. 20a). An excimer lamp ($\lambda = 172$ nm, UER20-172V, Ushio Inc.) was used as the light source. The monolayer irradiated with high energy photons with an energy of ca. 7.2 eV is photochemically decomposed. Details of this VUV photolithography we developed have been reported elsewhere [54-56]. In the second step, the monolayer resist was patterned by the AFM lithography (Fig. 20c). Prior to this second step, an LFM image of the photopatterned monolayer was acquired (Fig. 20b).

During imaging, the electric circuit is switched off and junction current is not allowed to flow, thereby protecting the monolayer resist from pattern drawing. An example is shown in Fig. 21a. Using the acquired image, the AFM probe is located at particular positions in order to draw additional patterns on the resist (Fig. 20c). In this research, the AFM-patterning was conducted in constant current mode with the sample substrate biased positively. Consequently, the pattern defined by the probe movement is transferred onto the monolayer. Finally, the sample is etched in an aqueous solution of the NH₄F/H₂O₂/H₂O solution to transfer

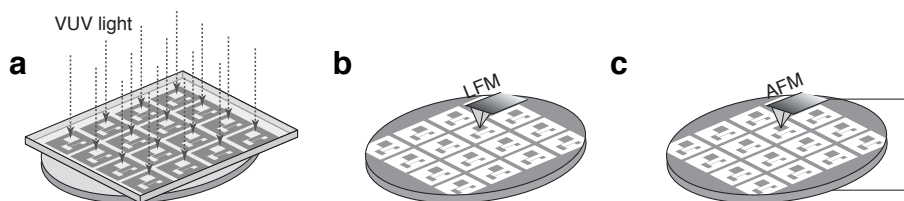


Figure 20. Schematic illustration of the integrated lithography. a) VUV-exposure of a monolayer resist on a substrate. b) LFM imaging of the VUV-exposed pattern. c) Probe alignment of the VUV-exposed pattern based on the LFM image and AFM patterning.

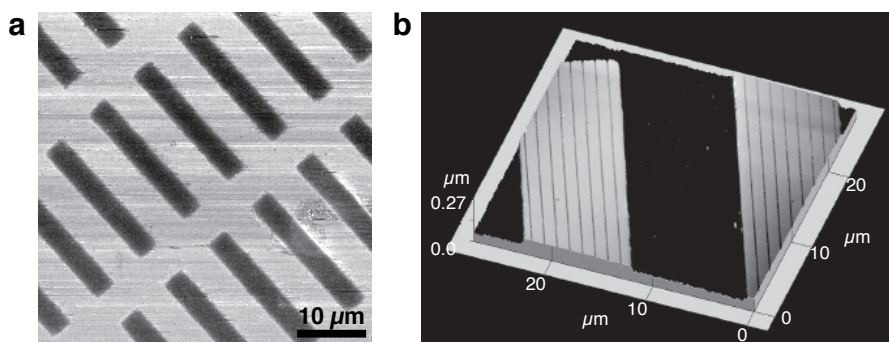


Figure 21. a) LFM image of the photopatterned ODS-Si sample surface. A microfabricated Si probe (Park Scientific Instruments, Ultralever UL20A) was used to acquire the image. b) FM image of an etched structure on a Si substrate patterned by the combined lithography. The ODS monolayer was exposed for 10 min with VUV light in order to print a photomask image. AFM patterning was conducted at a line drawing speed of $25 \mu\text{m/s}$ and a junction current of 2 nA using a microfabricated Si probe (Nanosensor, G2 T3-5 L125R). Etching was conducted for 3 min.

the photoprinted and probe-scanned patterns into the substrate Si.

An example of structures fabricated by the integrated lithography is shown in Fig. 21b. LFM imaging was applied for the pattern alignment. The wide $10 \mu\text{m}$ stripes were defined by photolithography. Fine grooves about 70 nm wide were successfully drawn on the wide stripes parallel to their direction. LFM was successfully applied to the imaging of the photoprinted pattern on the monolayer resist without its exposure or damage. Other scanning probe techniques, e.g., phase imaging, force modulation microscopy and surface potential microscopy, are also expected to be applicable to the pattern alignment, since these techniques enable to image VUV-patterned SAM samples distinctly as well as LFM [47,57].

5. Scanning probe chemical conversion

The SPM-based electrochemical modification of an organosilane SAM has been mainly focused on decomposition and elimination of molecules from the SAM so far. There have been a few reports describing chemical conversion of molecules consisting of SAMs [58-62] instead of eliminating the molecules. In order to construct molecular nanostructures as designed, such techniques are more important than the elimination processes.

In this section, we focus on chemical conversion of surface terminal functional groups on a SAM while its main part remains unmodified [63-65] and, furthermore, conversion of such surface terminating functional groups through scanning probe oxidation and reduction in a reversible manner [64,65]. Furthermore, Kelvin-probe force microscopy (KFM) is employed in order to elucidate chemical states of the modified SAMs, since KFM is a powerful means to study chemical and physical properties of the SAMs [57,66,67].

5-1. Anodic surface modification of ODS

An ODS-Si sample was modified using an AFM (Seiko Instruments Inc., SPA-300HV+SPI-3800N). First, the sample was modified by the AFM operated in the contact mode (C-AFM). A spiral-like pattern was drawn at $V_s = +10 \text{ V}$ and $v = 0.5 \mu\text{m/sec}$ in air with 40%RH. The modified sample surface was observed by KFM. A gold coated Si probe (SII Nanotechnology Inc., force constant = 1.8 N/m) was used both for the patterning and KFM imaging. Next, the ODS-Si sample was modified by the AFM operated in the intermittent contact mode (IC-AFM). An AFM probe was vibrated at a frequency slightly greater than its resonance and, consequently, intermittently touches a sample surface once in one vibration cycle. A Si probe (Nanosensor, force constant = $20 \sim 40 \text{ N/m}$, resonance frequency = 260 kHz, resistivity = $0.1 \sim 0.2 \Omega\text{cm}$) was used for the experiment. A similar spiral-like pattern was drawn on the sample at $V_s = +10 \text{ V}$ and $v = 0.5 \mu\text{m/sec}$ in air with 40%RH. The modified sample surface was observed by KFM as well. Finally, the ODS-Si sample was modified by the AFM operated in the non-contact mode (NC-AFM). In this mode, an AFM probe is vibrated at a frequency slightly smaller its resonance. A Si probe identical to that used in the IC-AFM experiment was used for this experiment.

Figures 22a and 22d are surface potential and topographic images, respectively, of a pattern fabricated by C-AFM simultaneously acquired by KFM. As can be seen in the potential image (Fig. 22a), the modified region shows a higher surface potential than the unmodified ODS monolayer. Furthermore, the probe-scanned, that is, current-injected, region, protrudes from the surrounding unmodified region. The protruding

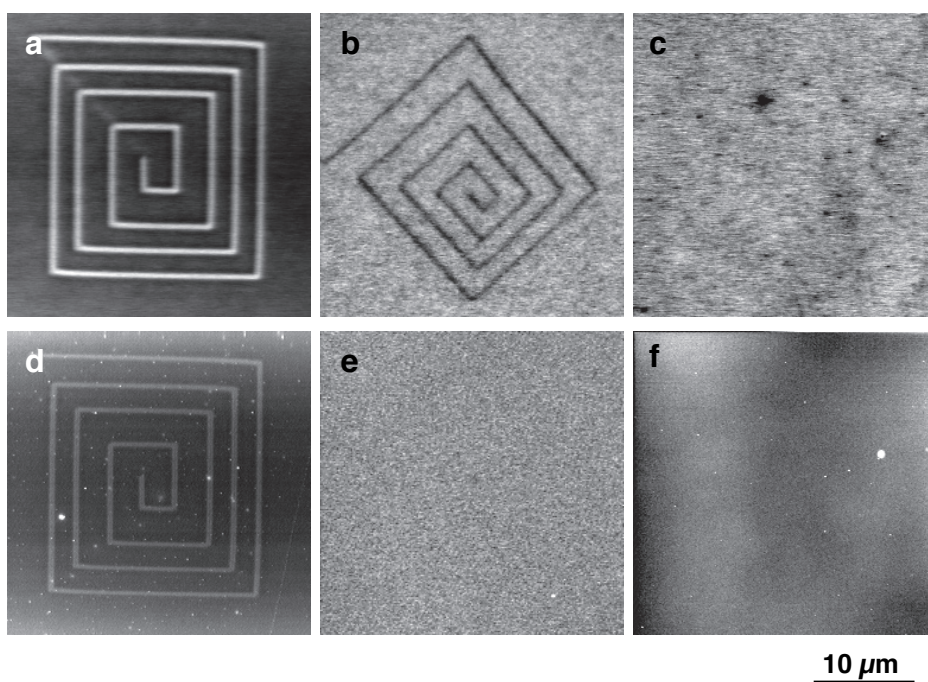


Figure 22. Modification of the ODS-Si sample using AFM. Surface potential images of the ODS-Si sample modified by C-AFM (a), IC-AFM (b) and NC-AFM (c). Topographic images of the ODS-Si sample modified by C-AFM (d), IC-AFM (e) and NC-AFM (f). Each image is $30\ \mu\text{m} \times 30\ \mu\text{m}$.

height is ca. 3 nm. As described in Section 4, due to anodic oxidation, the ODS monolayer was decomposed and removed from the probe-scanned region and the substrate Si was also anodized to silicon oxide resulting the protrusion formation due to the volume expansion accompanying the oxidation. Finally, the region became covered with silicon oxide which showed a higher surface potential than the ODS monolayer [57].

A clear pattern is seen in the KFM image as shown in Fig. 22b. The modified region where current had been injected by IC-AFM showed a lower surface potential than the unmodified ODS monolayer. However, any protrusions or depressions are recognizable in the topographic image as shown in Fig. 22e, indicating that, in the IC-AFM-scanned region, the ODS monolayer was not decomposed and the substrate Si was not anodized. Polar functional groups which attracted electrons and polarized negatively were generated on the ODS monolayer. It is most likely that this methyl(CH_3)-terminated SAM surface electrochemically oxidized to a carboxyl(COOH)-terminated surface.

No topographic and potential features appeared in the AFM and KFM images as shown in Figs. 22c and 22f, respectively. In NC-AFM, no water capillary was formed between the tip and sample. Accordingly, surface modification did not proceed. The actual contact of the AFM probe to the ODS-monolayer surface is crucial to attain surface modification through scanning probe electrochemistry.

The difference in the anodic oxidation behavior between C-AFM and IC-AFM can be explained as follows. In IC-AFM, current is injected to the ODS monolayer with an interval. Thus, the amount of the injected current is assumed to be too small to decompose the ODS monolayer and to anodize the substrate Si compared with that in C-AFM. Besides current density, the effective bias voltage applied to the sample is not constant but pulse-like in IC-AFM. The effective bias is applied to the sample during the probe is closed to the sample surface, thus, only a short time in one cycle. This may be the reason why the ODS monolayer surface was chemically modified by IC-AFM without forming any topographic features.

5-2. Reversible nanochemical conversion

By the vapor phase method described in Section 2, an amino-terminated SAM was prepared on Si substrates using p-aminophenyltrimethoxysilane [APhS, $\text{H}_2\text{N}(\text{C}_6\text{H}_4)\text{Si}(\text{OCH}_3)_3$] as a precursor. Chemical structures of APhS molecule and the corresponding SAM are shown in Fig. 23a. The surface modification experiments were conducted in air using the AFM in the contact mode with a gold-coated Si cantilever (SII nanotechnologies, Inc., force constant = 1.8 N/m). When biasing the substrate positively, anodic reactions, i.e., oxidation, are expected to proceed on the sample surface, while cathodic reactions, i.e., reduction, are expected to proceed on the sample surface when biasing it negatively.

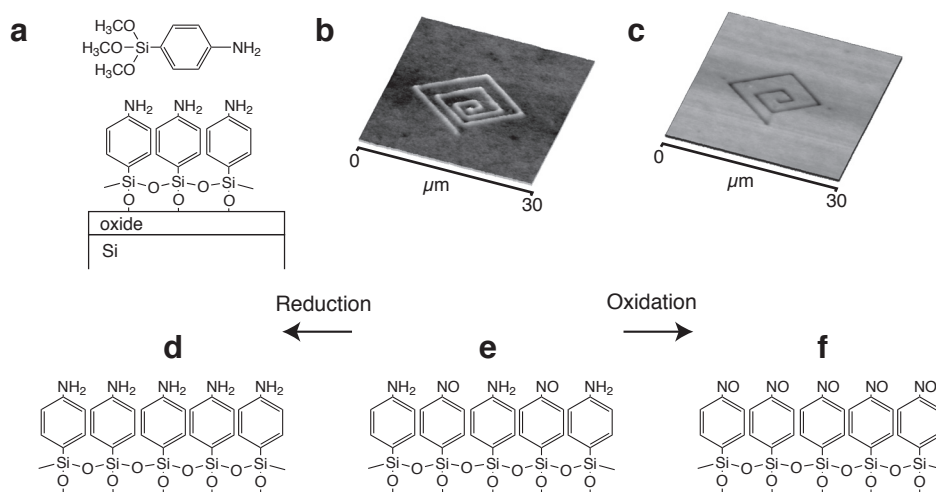


Figure 23. Chemical conversion of APhS-Si samples. a) Chemical structures of APhS molecule and APhS monolayer. b) KFM image of the APhS-Si modified by AFM-probe scanning with a cathodic sample bias at -3 V. c) KFM image of the APhS-Si modified by AFM-probe scanning with an anodic sample bias at +3 V. Chemical states of the APhS monolayer; d) reduced state, e) partially oxidized state and f) oxidized state.

Figures 23b and 23c show surface potential images of patterned regions on the APhS monolayer surface where had been scanned at $V_s = -3.0$ and $+3.0$ V, respectively, with $v = 100 \mu\text{m}/\text{sec}$. As clearly seen in these images, the probe-scanned regions have different surface potentials compared with that of the as-prepared APhS monolayer surface. By scanning with the negative sample bias voltage, a bright pattern possessing a surface potential 10 mV higher than the APhS monolayer had been formed, while, with the positive sample bias voltage, a dark pattern possessing a surface potential 20 mV lower than the as-prepared SAM surface had been formed. These surface potential images clearly demonstrate that certain chemical reactions proceeded on the SAM depending on the bias polarity. It is noteworthy that there have been no apparent topographic changes in the probe-scanned regions.

In an aqueous solution, amino (NH_2) groups can be electrochemically oxidized to nitroso (NO) groups, while NO groups can be electrochemically reduced to NH_2 groups as well. Since we have conducted the patterning experiment in air with 40%RH, a negligible amount of adsorbed water was presented on the sample surface. Electrochemistry with this adsorbed water is a plausible mechanism of the surface modification of the APhS monolayer. Thus, the reduced and oxidized states of the APhS monolayer fabricated in this study are considered to have NH_2 -terminated and NO-terminated surfaces, respectively, as illustrated in Figs. 23d and 23f. The NO-terminated monolayer surface is assumed to be polarized negatively, since NO groups attract electrons from the aromatic rings consisting of the SAM. Therefore, the surface potential of the SAM shifts toward the negative direction when terminated with NO groups. This is the reason why the probe-oxidized area showed lower surface potentials than the surrounding as-prepared SAM surfaces. On the other hand, the NH_2 -terminated surface is assumed to be polarized positively, since NH_2 -groups supply electrons to the aromatic rings. The NH_2 -terminated surface, that is, the reduced state of the APhS monolayer, is expected to show a higher surface potential than the oxidized surfaces.

The result, as shown in Fig. 23b, that the as-prepared APhS monolayer could be further reduced indicates that the SAM was considered to be in an incompletely reduced state. The as-prepared APhS monolayer was assumed to be partially oxidized. This is strange because the precursor molecules had been supplied as the reduced form, however, is explainable based on our preparation process. Since we employed a vapor phase method, APhS molecules were heated in the presence of oxygen molecules at a temperature of 373 K for one hour. This made some amount of the molecules to be oxidized resulting in the formation on the partially oxidized monolayer as illustrated in Fig. 23e.

In order to confirm our hypothesis, chemical nature of the probe-modified APhS monolayers were analyzed through a chemical labeling method. Samples modified by SPM-reduction and -oxidation were immersed in a solution of latex nano-particles whose surfaces had been modified with COOH groups. The pH of the solution was adjusted to be 4.0 in order to protonate NH_2 groups to NH_3^+ , while to deprotonate COOH groups to COO^- . Accordingly, the particles are expected to interact electrostatically with the amino-surface. Indeed, as confirmed by optical microscopy, the nanoparticles aggregated on the SPM-reduced regions while

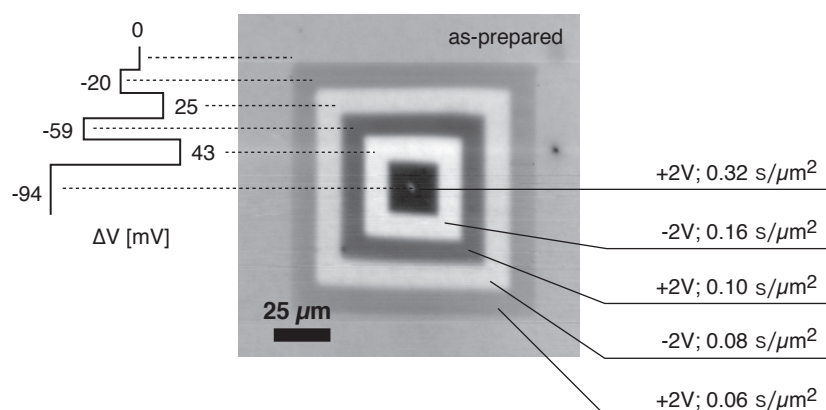


Figure 24. reversible scanning probe cchemical conversion of the APhs-Si saple surface. Surface potential contrasts to the potential of the as-prepared AphS monolayer surface and scanning densities are indicated in the figure.

the SPM-oxidized regions remained unadsorbed with the particles. Some of the nanoparticles adsorbed on the as-prepared SAM although its amount was smaller than that on the SPM-reduced regions. This result supports the assumption that the as-prepared SAM was partially oxidized.

Figure 24 shows an example of multiple overwriting with repeated oxidation and reduction. Dark and bright regions correspond to oxidized and reduced regions, respectively. First, a 100- μm square region was oxidized at $V_s = +2$ V. The oxidized region showed a surface potential 20 mV lower than the as-prepared APhS monolayer. Next, an 80- μm square region was reduced at $V_s = -2$ V resulting in the formation of the region whose surface potential was +25 mV vs. the as-prepared APhS monolayer. Then, 60- μm , 40- μm and 20- μm square regions were oxidized, reduced and oxidized in that order. Potentials of the regions were -59, +43 and -94 mV vs. the as-prepared APhS monolayer, respectively. Differences in the surface potentials among the oxidized regions and those among the reduced regions are ascribed to be dependent on scan density, that is, probe-scanning time per unit area as indicated in the figure. SPM-based electrochemical conversion of the APhS monolayer was demonstrated to be conducted reversibly. In addition, the degree of oxidation or reduction can be controlled with a scan density.

6. Chemical approach toward nanoscopic surface architecture

If a substance with chemical or physical properties different from those of the substrate material can be area-selectively deposited on patterns predefined by scanning probe lithography, nano-scale patterns of various functionalities can be fabricated. Patterned SAMs have been used as templates for the fabrication of minute structures made up of a variety of materials through various chemical modifications [8, 68-72]. Nanopatterns fabricated on organosilane SAMs by means of scanning probe lithography is applicable as nanotemplates as well. In this section, we describe this approach for constructing nanostructures in our nanoscopic surface architecture strategy [73-75].

In the first demonstration [75], we show the arrangement of organic molecules for regulating surface potentials at the spatial resolution in nanometer scale. A nanotemplate is fabricated on an ODS-Si sample (Fig. 25a) by the AFM lithography. Figures 25a and 25b show topographic and surface potential images of the nanopatterned ODS-Si sample. The probe-scanned trace is clearly observable in the both images. As can be seen in this KFM image, the surface potential of the current-injected lines 50 mV higher than that of the surrounding surface where had not been current-injected. In addition, as can be seen in the topographic image shown in Fig. 25a, the scanned lines are slightly protruded from the surrounding unscanned area, owing to volume expansion which accompanied the anodization of the substrate Si appeared to occur after the removal of ODS monolayer. Its topographic height and width are 1 ~ 1.5 nm and ca. 90 nm, respectively.

As demonstrated in the previous sections, the regions where the monolayer is electrochemically removed by scanning probe lithography are hydrophilic, since they preferentially wetted with water. The surface of the lines is most likely terminated with OH groups. Thus, the line regions on the nanotemplate are expected to become once again reactive to organosilane molecules. It is possible to fix a different type of organosilane molecule onto the probe-scanned, therefore, current-injected lines. The unscanned regions are unreactive due to the termination with the ODS monolayer. Consequently, organosilane molecules other than alkyl groups can be attached onto the predefined patterns. In order to demonstrate this hypothesis, the fabricated nanotemplate was then treated with a fluoroalkylsilane (FAS), that is, heptadecafluoro-1,1,2,2-tetrahydro-

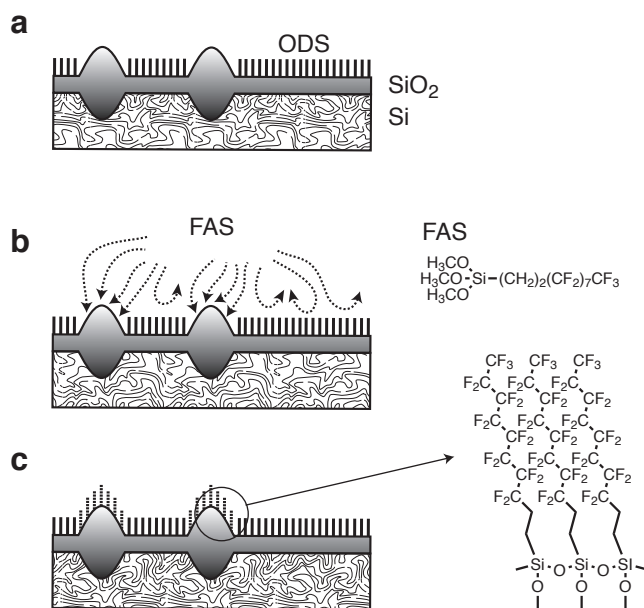


Figure 25. Schematic diagram for preparation of molecular nanostructures. a) Nanotemplate: an ODS-Si sample on which a nanopattern has been drawn by the AFM lithography. b) Area-selective FAS deposition on the current-injected regions. c) the fabricated ODS/FAS nanostructure.

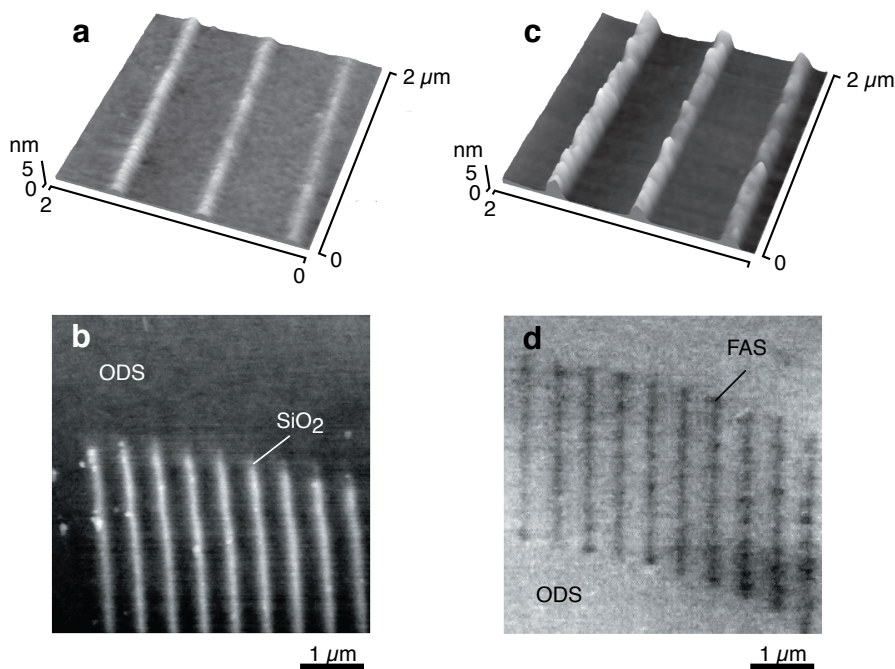


Figure 26. Topographic and surface potential images of the nanotemplate and the fabricated nanostructure with ODS and FAS. a) Topographic AFM image of the nanotemplate and its KFM image. Patterning had been conducted in air at an applied bias voltage of 10 V with an probe moving speed of 0.1 μm/sec. c) Topographic AFM image of the FAS-treated template surface and d) its KFM image. The sample had been treated with FAS vapor for 3 hours at a temperature of 150 °C. These KFM images were acquired at a scan rate of 0.1 Hz using a gold-coated Si probe with a force constant of 2.8 N/m.

decyl-1-trimethoxysilane (Fig. 26b), by the vapor phase method described in Section 2.

After the sample had been treated with FAS, it was observed again by AFM and KFM. The probe-scanned lines became more protruded before the FAS treatment. Its topographic height from the surrounding ODS monolayer is 2 ~ 3 nm. The increase in height from Fig 26a is 1 ~ 1.5 nm corresponding to the thickness of the FAS monolayer. Figure 26d shows a KFM image of the FAS-treated sample. It surface potential contrast is inverted compared with the KFM image acquired before the FAS-treatment

(Fig. 26b). The probe scanned lines have become to show a lower surface potential than the surrounding unscanned ODS monolayer. The value of this potential contrast was ca. 30 mV. The surface potential of the FAS monolayer was reported to be ca. 170 mV lower than that of ODS monolayer due to the FAS monolayer's large dipole moment directing from its top surface to the bottom generated with the electron negativity of fluorine atoms [76].

From these experimental results on topography and surface potential, we concluded that FAS molecules were area-selectively fixed onto the probe-scanned lines on the ODS monolayer. The origin of insufficient potential contrast of 30 mV compared to that between ODS and FAS-SAMs is probably ascribable to the imperfection or disorder of the monolayer, since the total dipole moment of a SAM is dependent on its molecular structures such as packing density [66]. Close inspection of Fig. 26c shows that the line surface had a some roughness compared with that of the lines before the FAS-treatment as shown in Fig. 1a, indicating that the FAS-SAM formed on the probe-scanned lines was disordered somewhat.

In the second demonstration of nanoscopic surface architecture [73,74], the spatial arrangements of nanoscopic objects such as particles and protein molecules are shown. As shown in Fig. 27, instead of the FAS-monolayer, an amino-terminated monolayer is formed on the nanotemplate which served as a nanotemplate with a different chemical affinity.

TMS-Si samples patterned by the STM lithography were washed in distilled water and ethanol, in that order, and dried by N₂ blow. Next, they were immersed in a fresh solution of 1 vol.% APS, 4 vol.% CH₃COOH and 4 vol.% H₂O in methanol for 5 min. After this, the samples were rinsed in methanol twice and then in distilled water. Finally, one of the APS-treated sample was immersed for 30 min in 50 ml of morpholinoethane sulfonic acid buffer (MES; 50 mM, adjusted to pH6.5 by adding aq-NH₄OH solution), and 0.2 ml of an aqueous suspension of aldehyde-modified latex particles (Molecular Probes, L-5401, 2% solids in H₂O, diameter = 29 nm ± 20.1%). These samples were again rinsed in distilled water and then blown dry. The AFM image as shown in Fig. 28a show the aldehyde-modified latex particles deposited on the tip-scanned area. There were no particles on the surrounding unscanned area. Since the thickness of the deposited-particle layer is nearly equal to the average diameter of the particles, this particle layer is thought to consist of a monolayer of the particles. It is known that an aldehyde group reacts with an amino group to form a chemical bonding as shown by eq. (1):



The particles were immobilized by this reaction between the amino groups in the APS molecules and the aldehyde groups on each particle. Therefore, APS molecules chemisorbed area-selectively onto the tip-

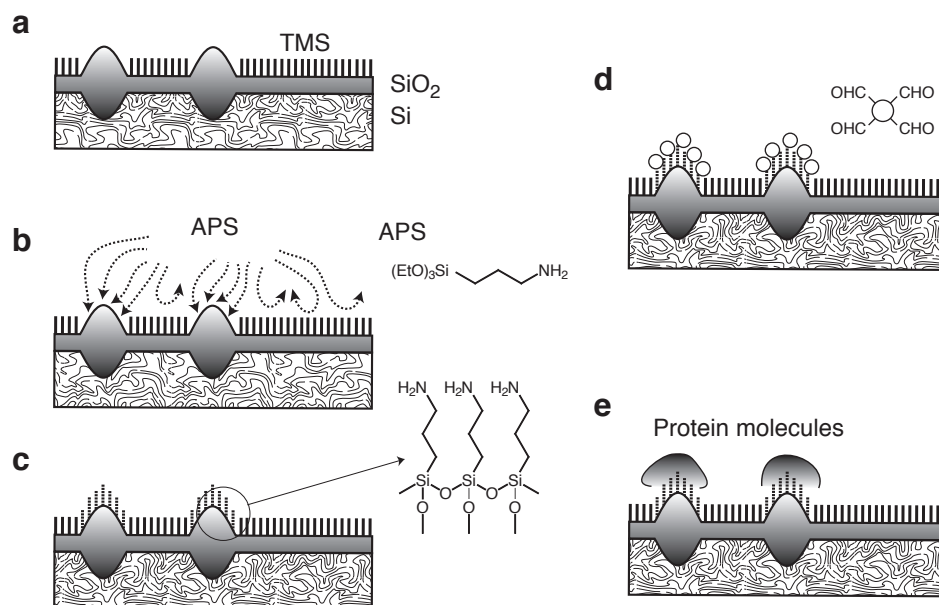


Figure 27. Schematic diagram of nanoscopic surface architecture a) Patterned TMS-Si sample by scanning probe lithography. b) Area-selective APS deposition on the current-injected regions. c) the fabricated APS/TMS nanostructure. Assembling aldehyde-modified nanoparticles (d) or protein molecules (e) onto the amino-terminated nanotemplate.

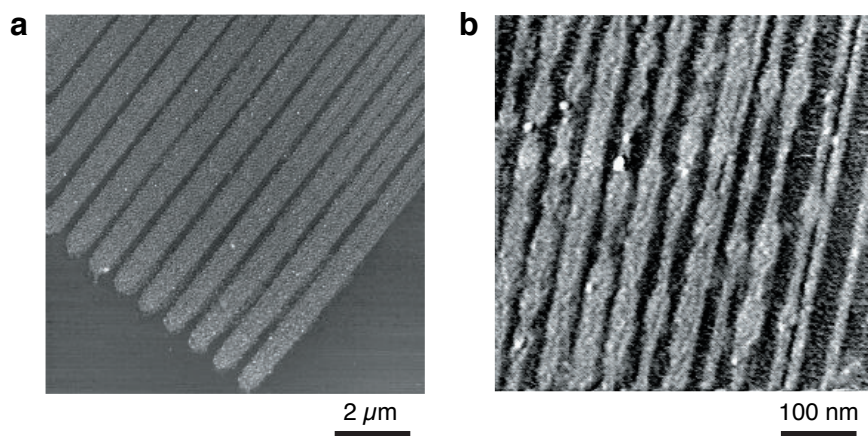


Figure 28. Assembled structures. a) AFM image of the nanoparticles selectively arranged onto the amino-terminated area. The template was prepared by the STM lithography at $V_s = +5.0$ V and $v = 0.2 \mu\text{m}/\text{sec}$ in N_2 with 80%RH. The size of image is $10 \mu\text{m} \times 10 \mu\text{m}$. b) Phase lag image of an APS-treated sample modified with HRP. The APS-treated sample was immersed for 30 min in 2.5 ml of a 50% glutaraldehyde aq-solution (Kishida Chemical) diluted with 100 ml of phosphate buffered saline (Biowhittaker, PBS) and then rinsed in pure water. Next, the samples were soaked into a 1 mg HRP (Sigma) solution in 5 ml PBS.

scanned area, resulting in its termination with amino groups. In addition, we confirmed that, after the APS treatment, the tip-scanned area could not be etched in the $\text{NH}_4\text{F}/\text{H}_2\text{O}_2/\text{H}_2\text{O}$ solution. A protective coating of APS molecules had formed on the tip-scanned area.

Such an amino-terminated template can be applied to assembling not only nanoparticles, but also a variety of organic molecules and biomolecules, such as proteins (Fig. 26e), by using a suitable cross-linker between an amino group and a molecule. An example is shown in Fig. 27e. protein molecules (horseradish peroxidase, HRP, Sigma) were selectively assembled onto an APS-modified template using glutaraldehyde as a cross-linker between the amino groups of the APS monolayer and those of HRP. Figure 28b shows a phase contrast image which maps softness of a sample surface. It has been reported that adsorbed organic molecules showed larger phase lag than a rigid substrate due to the differences in softness and/or viscosity between them [77]. As clearly seen the image, there is a larger phase lag on the amino-terminated area compared to the surrounding region where there were no adsorbates. In addition, the region protruded $4 \sim 5$ nm from the surrounding area. It is most likely that the protein molecules were assembled area-selectively onto the patterned APS monolayer defined by scanning probe lithography and molecular self-assembly.

7. Conclusion

In this review, our research on the surface modification of organosilane SAMs based on SPM and its applications to nanolithography have been reported. We have modified the SAMs formed on Si substrates by locally injecting current into the sample surfaces from the SPM tip. The best patterning resolution of $10 \sim 20$ nm has been attained. Although, both, STM and AFM are applicable, a conductive probe, e.g., metal-coated one or that made from heavily doped Si, is used for AFM-based nanopatterning. The surface modification proceeded only when current was injected in an humid atmosphere, but did not occur in vacuum. Thus, the surface modification chemistry was ascribed to electrochemical reactions related to adsorbed water, i.e. that is, scanning probe electrochemistry.

Advantages of STM in scanning probe lithography are that STM is operated based on current flowing at the STM tip/sample junction. The current flowing through the junction, therefore, the electrochemical reactions used for surface modification, is readily controllable. However, STM requires an electrical conductivity of a sample to some extent. Thus, in our case, the ODS-Si sample is hard to be applied for the sample of STM lithography.

On the contrary, the position and motion of the AFM probe is operated independently of the origin of surface modification, that is, current. AFM is applicable to pattern a relatively low conductive sample surface. Consequently, we can use the multilayer resist film, which mainly consists of a thin a-Si layer and thus has a very low conductivity, to scanning probe lithography for nanofabrication of insulator. Other advantages of the AFM lithography are as follows. Much higher patterning speeds are available than the STM lithography. We have succeeded in patterning at a speed in the range of mm/sec by installing a current regulating

system to the AFM. The AFM-based scanning probe lithography has compatibility with photolithography. It is crucial abilities of AFM for in-situ characterization and imaging of fabricated nanopatterns without injecting current to the sample, namely, without modifying the nanopatterns at all, to integrate AFM lithography and photolithography.

In addition to degrading and removing SAMs from the substrates by the use of anodic reactions, we have successfully demonstrated the chemical conversion of surface-terminating functional groups on SAMs by the use of both anodic and cathodic reactions. By extending this method, we have succeeded in reversibly converting the SAM surface from oxidized states to reduced states and vice versa, when a proper material system is selected. By manipulating both oxidation and reduction reactions by SPM, the construction of organic molecular nanostructures will come true in a more sophisticated manner.

Finally, we have demonstrated the nanoscopic surface architecture based on scanning probe electrochemistry and molecular self-assembly. The two-step surface modification presented here, i.e., local removal of an organosilane monolayer through scanning probe lithography followed by the selective chemisorption of a second monolayer of organosilane molecules, provides a method for fabricating patterned sites with various chemical reactivities and, therefore, shows promise in the preparation of templates for constructing molecular assemblies. Using such chemically reactive patterns as templates, nanostructured assemblies of molecular species such as fluorescent molecules, redox reagents, catalysts and biologically active species can be synthesized. This technique will contribute to the future realization of nano chemical/biochemical systems and novel molecular devices.

References

- 1 H. Rohrer, *Jpn. J. Appl. Phys.* **32** 1335 (1993).
- 2 P. Avoris, *Acc. Chem. Res.* **28** 95 (1995).
- 3 H. Sugimura and N. Nakagiri, *Jpn. J. Appl. Phys.* **34** 3406 (1995).
- 4 R. M. Nyffebegger and R. M. Penner, *Chem. Rev.* **4** 1195 (1997).
- 5 C. F. Quate, *Surf. Sci.* **386** 259 (1997).
- 6 H. T. Soh, K. W. Guarini and C. F. Quate, "*Scanning Probe Lithography* (Kluwer Academic Publishers, Boston, 2001)".
- 7 K. Sattler, *Jpn. J. Appl. Phys.* **42** 4825 (2003).
- 8 D. Wouters and U. S. Schubert, *Angew. Chem. Int. Ed.* **43** 2480 (2004).
- 9 A. Ulman, "*An Introduction to Ultrathin Organic Films From Langmuir-Blodgett to Self-Assembly* (Academic Press, Boston, 1991)".
- 10 J. Sagiv, *J. Am. Chem. Soc.* **102** 92 (1980).
- 11 S. R. Wasserman, Y. T. Tao and G. M. Whitesides, *Langmuir* **5** 1074 (1989).
- 12 H. Sugimura and N. Nakagiri, *J. Photopolym. Sci. Technol.* **10** 661 (1997).
- 13 H. Sugimura, A. Hozumi, T. Kameyama and O. Takai, *Surf. Interf. Anal.* **34** 550 (2002).
- 14 "*Speciality Silicon Reagents, Third Edition*, Petrarch Systems, 1985".
- 15 M. A. McCord and R. F. W. Pease, *J. Vac. Sci. Technol. B* **4** 86 (1986).
- 16 M. A. McCord and R. F. W. Pease, *J. Vac. Sci. Technol. B* **6** 293 (1988).
- 17 E. A. Dobisz and C. R. K. Marrian, *Appl. Phys. Lett.* **58** 2526 (1991).
- 18 H. C. Day, D. R. Allee, R. George and V. A. Burrows, *Appl. Phys. Lett.* **62** 1629 (1993).
- 19 L. Stockman, G. Neuttiens, C. Van Haesendonck and Y. Bruynseraede, *Appl. Phys. Lett.* **62** 2935 (1993).
- 20 C. B. Ross, L. Sum and R. M. Crooks, *Langmuir* **9** 632 (1993).
- 21 M. J. Lercel, G. F. Redinbo, H. G. Craighead, C. W. Sjeen and D. L. Allara, *Appl. Phys. Lett.* **65** 974 (1994).
- 22 J. K. Schoer, F. P. Zamborini and R. M. Crooks, *J. Phys. Chem.* **100** 11086 (1996).
- 23 C. R. K. Marrian, F. K. Perkins, S. L. Brandow, T. S. Koloski, E. A. Dobisz and J. M. Calvert, *Appl. Phys. Lett.* **64** 390 (1994).
- 24 F. K. Perkins, E. A. Dobisz, S. L. Brandow, T. S. Koloski, J. M. Calvert, K. W. Rhee, J. E. Kosakowski and C. R. K. Marrian, *J. Vac. Sci. Technol. B* **12** 3725 (1994).
- 25 H. Sugimura and N. Nakagiri, *Langmuir* **11** 3623 (1995).
- 26 H. Sugimura and N. Nakagiri, *J. Vac. Sci. Technol. A* **14** 1223 (1996).
- 27 H. Sugimura, K. Okiguchi and N. Nakagiri, *Jpn. J. Appl. Phys.* **35** 3749 (1996).
- 28 H. Sugimura, K. Okiguchi, N. Nakagiri and M. Miyashita, *J. Vac. Sci. Technol. B* **14** 4140 (1996).
- 29 H. Sugimura, T. Hanji, K. Hayashi and O. Takai, *Ultramicroscopy* **91** 221 (2002).
- 30 H. Sugimura, T. Uchida, N. Kitamura and H. Masuhara, *Jpn. J. Appl. Phys.* **32** L553 (1993).
- 31 H. C. Day and D. R. Allee, *Appl. Phys. Lett.* **62** 2691 (1993).
- 32 M. Yasutake, Y. Ejiri and T. Hattori, *Jpn. J. Appl. Phys.* **32** L1021 (1993).
- 33 H. Sugimura, T. Uchida, N. Kitamura and H. Masuhara, *J. Phys. Chem.* **98** 4352 (1994).

- 34 H. Sugimura, H., N. Kitamura and H. Masuhara, *Jpn. J. Appl. Phys.* **33** L143 (1994).
- 35 E. S. Snow and P. M. Campbell, *Appl. Phys. Lett.* **64** 1932 (1994).
- 36 J. A. Dagata, J. Schneir, H. H. Harary, C. J. Evans, M. T. Postek and J. Bennett, *Appl. Phys. Lett.* **56** 2001 (1990).
- 37 L. A. Nagahara, T. Thundat and S. M. Lindsay, *Appl. Phys. Lett.* **57** 270 (1990).
- 38 R. L. McCarley, S. A. Hendricks and A. J. Bard, *J. Phys. Chem.* **96** 10089 (1992).
- 39 L. J. M. Schlangen, L. K. Koopal, M. A. C. Stuart, J. Lyklema, M. Robin and H. Toulhoat, *Langmuir* **11** 1701 (1995).
- 40 S. W. Park, H. T. Soh, C. F. Quate and S. Park, *Appl. Phys. Lett.* **67** 2415 (1995).
- 41 J. P. Bourgoin, R. V. Sudiwala and S. Palacin, *J. Vac. Sci. Technol. B* **14** 3381 (1996).
- 42 H. Sugimura and N. Nakagiri, *Nanotechnology* **8** A15 (1997).
- 43 E. S. Snow, P. M. Campbell and F. K. Perkins, *Appl. Phys. Lett.* **75** 1476 (1999).
- 44 M. Mullenborn, K. Birkelund, F. Grey and S. Madsen, *Appl. Phys. Lett.* **69** 3013 (1996).
- 45 H. Sugimura and N. Nakagiri, *Jpn. J. Appl. Phys.* **36** L968 (1997).
- 46 A. Boisen, K. Birkelund, O. Hansen, and F. Grey, *J. Vac. Sci. Technol. B* **16** 2977 (1988).
- 47 H. Sugimura and N. Nakagiri, *Appl. Phys. A* **66** S427 (1998).
- 48 E. S. Snow and P. M. Campbell, *Science* **270** 1639 (1995).
- 49 T. Yasue, H. Koyama, T. Kato and T. Nishioka, *J. Vac. Sci. Technol. B* **15** 614 (1997).
- 50 K. Hayashi, H. Sugimura and O. Takai, *Jpn. J. Appl. Phys.* **40** 4344 (2001).
- 51 M. Fujihira, D. Aoki, Y. Okabe, H. Takano, H. Hokari, J. Frommer, Y. Nagatan and F. Sakai, *Chem. Lett.* 499 (1996).
- 52 H. Sugimura, O. Takai and N. Nakagiri, *J. Vac. Sci. Technol. B* **17** 1605 (1999).
- 53 H. Sugimura and N. Nakagiri, *Jpn. J. Appl. Phys.* **36** L968 (1997).
- 54 H. Sugimura, K. Ushiyama, A. Hozumi and O. Takai, *Langmuir* **16** 885 (2000).
- 55 L. Hong, H. Sugimura, T. Furukawa and O. Takai, *Langmuir* **19** 1966 (2003).
- 56 L. Hong, H. Sugimura, O. Takai, N. Nakagiri and M. Okada, *Jpn. J. Appl. Phys.* **42** L394 (2003).
- 57 K. Hayashi, N. Saito, H. Sugimura, O. Takai and N. Nakagiri, *Ultramicroscopy* **91** 151 (2002).
- 58 R. Maoz, S. R. Cohen and J. Sagiv, *Adv. Mater.* **11** 55 (1999).
- 59 R. Maoz, E. Frydman, S. R. Cohen and J. Sagiv, *Adv. Mater.* **12** 424 (2000).
- 60 W. T. Müller, D. L. Klein, T. Lee, J. Clarke, P. M. McEuen and P. G. Schultz, *Science* **268** 272 (1995).
- 61 C. Blackledge, D. A. Engebretson and J. D. McDonald, *Langmuir* **16** 8317 (2000).
- 62 N. Saito, N. Maeda, H. Sugimura and O. Takai, *Langmuir* **20** 5182 (2004).
- 63 H. Sugimura, N. Saito, K. Hayashi, N. Maeda and O. Takai, *AIP Conference Proceedings* **696** 150 (2003).
- 64 H. Sugimura, *Jpn. J. Appl. Phys.* **43** 4477 (2004).
- 65 H. Sugimura, N. Saito, S. H. Lee and O. Takai, *J. Vac. Sci. Technol. B* **22** L44 (2004).
- 66 H. Sugimura, K. Hayashi, N. Saito, N. Nakagiri and O. Takai, *Appl. Surf. Sci.* **188** 403 (2002).
- 67 K. Hayashi, N. Saito, H. Sugimura, O. Takai and N. Nakagiri, *Langmuir* **18** 7469 (2002).
- 68 W. J. Dressick and J. M. Calvert, *Jpn. J. Appl. Phys.* **32** 5829 (1993).
- 69 A. Kumar, N. L. Abbott, E. Kim, H. A. Biebuyck and G. M. Whitesides, *Acc. Chem. Res.* **28** 219 (1995).
- 70 J. H. Fendler, *Chem. Mater.* **13** 3196 (2001).
- 71 S. Krämer, R. R. Fuieler and C. B. Gorma, *Chem. Rev.* **103** 4367 (2003).
- 72 R. K. Smith, P. A. Lewis and P. S. Weiss, *Prog. Surf. Sci.* **75** 1 (2004).
- 73 H. Sugimura and N. Nakagiri, *J. Vac. Sci. Technol. B* **15** 1394 (1997).
- 74 H. Sugimura and N. Nakagiri, *J. Am. Chem. Soc.* **119** 9226 (1997).
- 75 H. Sugimura, T. Hanji, K. Hayashi and O. Takai, *Adv. Mater.* **14** 524 (2002).
- 76 H. Sugimura, K. Hayashi, N. Saito, O. Takai and N. Nakagiri, *Jpn. J. Appl. Phys.* **40** 4373 (2001).
- 77 J. Tamayo and R. García, *Langmuir* **12** 4430 (1996).

Version 1.6 (July 30, 2005)